THE ASTROPHYSICAL JOURNAL, 420:756–771, 1994 January 10

INTERSTELLAR CARBON MONOXIDE TOWARD ζ OPHIUCHI[1]

DAVID L. LAMBERT,[2] YARON SHEFFER,[2] RONALD L. GILLILAND,[3] AND S. R. FEDERMAN[4]

Received 1993 May 17; accepted 1993 July 8

ABSTRACT

Interstellar CO A–X bands in the spectrum of ζ Oph were recorded at high S/N with grating G160M of the Goddard High Resolution Spectrograph on the *Hubble Space Telescope*. Isotopic fractionation of CO is severe: $^{12}CO/^{13}CO = 167$, $C^{16}O/C^{18}O \simeq 1550$ and $C^{16}O/C^{17}O > 5900$ are found where $^{12}C/^{13}C = 70$, $^{16}O/^{18}O = 500$, and $^{16}O/^{17}O = 2600$ are observed or expected. Standard models of the ζ Oph cloud predict $^{12}CO/^{13}CO \lesssim 70$. The higher observed ratio suggests that photodissociation of CO, not the isotopic charge exchange reaction ($^{13}C^+ + CO \leftrightarrow {}^{12}C^+ + {}^{13}CO$), is the dominant influence on the $^{12}CO/^{13}CO$ ratio.

Subject headings: ISM: abundances — ISM: molecules — stars: individual (ζ Ophiuchi)

1. INTRODUCTION

Absorption line spectroscopy of diffuse interstellar clouds is experiencing a renaissance initiated by the *Hubble Space Telescope* and its Goddard High-Resolution Spectrograph (GHRS). Carbon monoxide, an abundant molecule in diffuse interstellar clouds, is playing a part in the renaissance thanks to the molecule's ultraviolet electronic transitions $A\,^1\Pi$–$X\,^1\Sigma^+$ and $B\,^1\Sigma^+$–$X\,^1\Sigma^+$. In our previous paper (Sheffer et al. 1992, hereafter Paper I) on interstellar CO A–X bands seen in the spectrum of the bright star ζ Oph, we reported on the significant isotopic fractionation of CO: $^{12}CO/^{13}CO = 150 \pm 27$ where the true ratio, which is presumed to be provided by optical observations of the molecular ions $^{12}CH^+$ and $^{13}CH^+$, is $^{12}C/^{13}C = 70 \pm 3$ (Stahl et al. 1989; Crane, Hegyi, & Lambert 1991; Stahl & Wilson 1992).

Isotopic fractionation of CO was attributed to photodissociation by ultraviolet radiation. Since CO is photodissociated primarily by line radiation, ^{13}CO is destroyed preferentially because the more abundant ^{12}CO molecules are self-shielded to a greater extent. Amelioration of the effects of photodissociation occurs through the isotopic exchange reaction $^{13}C^+ + {}^{12}CO \leftrightarrow {}^{12}C^+ + {}^{13}CO$ which, in the absence of photodissociation, would ensure that $^{12}CO/^{13}CO < {}^{12}C/^{13}C$. Since the observed fractionation is of the opposite sense, we concluded that the diffuse clouds hosting the CO molecules are of low density and temperature, i.e., $n_H = n(H) + 2n(H_2) \leq 100$–$200\ cm^{-3}$ at $T \sim 50$ K.

In this paper, fractionation of CO in clouds along the line of sight to ζ Oph is reexamined using new GHRS spectra. Owing to the unavailability of the echelle ECH-A, the new observations were made at the lower resolution ($R = \lambda/\Delta\lambda = 15{,}000$–$20{,}000$) provided by the grating G160M. The rotational structure of the CO bands, which was well resolved with the echelle spectra discussed in Paper I, is but partially resolved in the new spectra. This potential loss of information has been offset by the high signal-to-noise (S/N) ratio of the new spectra: S/N ≃ 900 but only S/N ≃ 70 for the echelle spectra used in Paper I. Thanks to the high S/N, the new spectra provide novel information on the excitation temperatures for the lowest rotational levels of CO's ground vibrational state, and they reveal a difference between the shapes of the curves of growth of ^{12}CO and ^{13}CO that affects determinations of the ratio of the ^{12}CO and ^{13}CO column densities from empirical curves of growth; both of the earlier attempts to determine this ratio (Wannier, Penzias, & Jenkins 1982, hereafter WPJ; Paper I) assumed that the shape of the curve of growth was independnet of the isotopic flavor of CO. We offer an interpretation of the likely origin of the observed difference and rederive the $^{12}CO/^{13}CO$ ratio. This ratio and the excitation temperatures are related to the gas density (n_H) and the kinetic temperature of the two molecular components along the line of sight to ζ Oph.

2. OBSERVATIONS AND REDUCTIONS

Our series of observations of ζ Oph was designed to provide spectra of high S/N ratio such that the isotopic ratios $^{12}C^{16}O/^{13}C^{16}O$, $^{12}C^{16}O/^{12}C^{18}O$, and perhaps, $^{12}C^{16}O/^{12}C\,^{17}O$ could be estimated reliably or interesting lower limits established. The original intent to use the highest possible spectral resolution ($R = 90{,}000$) was frustrated when use of the echelle with the "blue" Digicon (ECH-A) was curtailed. Fortunately, grating G160M with the "red" Digicon provides an adequate resolution. Our goal of high S/N was not compromised. The virtues of a S/N = 900 are amply demonstrated here.

Our choice of wavelength intervals recognized that the large ratio of the $^{12}C^{16}O$ and $^{13}C^{16}O$ column densities means that a weak unsaturated $^{13}C^{16}O$ v'–band is accompanied by a very saturated $^{12}C^{16}O$ v'–0 band and, hence, the ratio of the column densities cannot be derived reliably from observations of a single band. Fortunately, the A–X system has vibrational bands with a wide range of $f(v', v'')$-values such that a weak $^{12}C^{16}O$ band of high v' can be found with approximately the same equivalent width as a $^{13}C^{16}O$ band with a larger $f(v', v'')$-value. Provided that the relative $f(v', v'')$-values are known, the desired ratio of the column densities is obtainable from observations of low v' and high v' bands. With the 40 Å bandpass provided by G160M in single exposure, it proved possible to capture two bands in one observation. Observations were

[1] Based on observations obtained with NASA/ESA *Hubble Space Telescope* through the Space Telescope Science Institute, which is operated by the Association of Universities for Research in Astronomy, Inc., under NASA Contract NASA-26555.

[2] Department of Astronomy, University of Texas, Austin, TX 78712.

[3] Space Telescope Science Institute, 3700 San Martin Drive, Baltimore, MD 21218.

[4] Department of Physics and Astronomy, University of Toledo, Toledo, OH 43606.

TABLE 1

OBSERVATION SUMMARY TABLE

λ_C[a] (Å)	Rootname[b]	UT[c] (1992)	Counts per Pixel[d]	T_{exp}[e] (s)
1463.7.....	z0x20108	112.863	87,763	1305.6
1464.8.....	z0x20109	112.881	163,920	1305.6
1462.6.....	z0x2010b	112.939	162,594	1305.6
1466.8.....	z0x2010c	113.001	160,800	1305.6
1461.0.....	z0x2010e	113.068	162,744	1305.6
1471.0.....	z0x2010f	113.136	158,368	1305.6
1353.1.....	z0x2010h	113.187	52,113	326.4
1335.0.....	z0x2010i	113.206	49,991	326.4
1357.9.....	z0x2010j	113.211	50,473	326.4
1271.1.....	z0x2010k	113.217	47,313	326.4
1273.0.....	z0x2010m	113.256	49,253	326.4
1275.9.....	z0x2010n	113.262	51,666	326.4

[a] Central wavelength in Å of spectra.

[b] Unique name for data set in the *HST* archive.

[c] UT time (day of year and decimal day of year 1992) at start of exposure.

[d] Total counts in one pixel (one quarter diode) summed over all subexposures. The telescope was repositioned by 0.″125 to center the star in the SSA after the z0x20108 exposure. All stellar data were acquired with STEP-PATT = 5 in which subspectra are acquired at 1/4 diode magnetic deflections. Background spectra are built up using 6% of the total integration time.

[e] Total exposure time in seconds. Exposures for z0x201o[8-f] used three repeats yielding subexposures of 435.2 s. All stellar exposures used FP-SPLIT = 4 further reducing the time per lowest level exposure by another factor of 4. Thus the longest period of time spent building up a single data group was 108.8 s.

made at central wavelengths of 1273, 1355, and 1465 Å: see Table 1 for a log of the observations. Portions of these spectra showing the six observed CO v'-0 bands are illustrated in Figures 1 to 3 (after the reductions discussed below). Interstellar features not identified as due to CO are atomic lines which are discussed by Federman et al. (1993).

The error budget for GHRS spectra consists of three primary terms: (1) an irreducible term from Poisson statistics on the object spectrum; (2) Poisson statistics on the accumulated background from the 0.01 count per second per diode dark noise; and (3) an irregular photocathode granularity, or flat-field error. In our spectra with object count rates of typically 500 Hz per diode the background noise is unimportant. Photocathode granularity, or fixed-pattern noise, has an amplitude of typically 0.5% on the GHRS Side 2 but ranges occasionally to features of several percent that can mimic spectral lines in general shape. Fixed-pattern noise is normally controlled through use of FP-SPLIT observations in which spectra are aquired at four successive carousel positions, resulting in independent spectra for which any photocathode features remain fixed in pixel position while stellar features move relative to the pixel coordinates. In principle, it is therefore easy to discriminate between stellar signals and photocathode blemishes.

In practice the FP-SPLIT solution does not work well if the stellar spectrum contains lines separated by the FP-SPLIT offsets, or if regions of the spectrum are dominated by strong aborption over a width comparable to the full offset range. For example (see Fig. 3), the complex of lines near 1261 and 1280 Å have repeated structure at separations comparable to offsets with FP-SPLIT. A direct solution for possible photocathode features in such a case would be unstable, resulting in a very noisy solution. For this project we have utilized a super-FP-SPLIT procedure in which several separate FP-SPLIT sets are acquired with sufficiently large shifts between them to exchange continuum and line-rich regions. Therefore an expo-

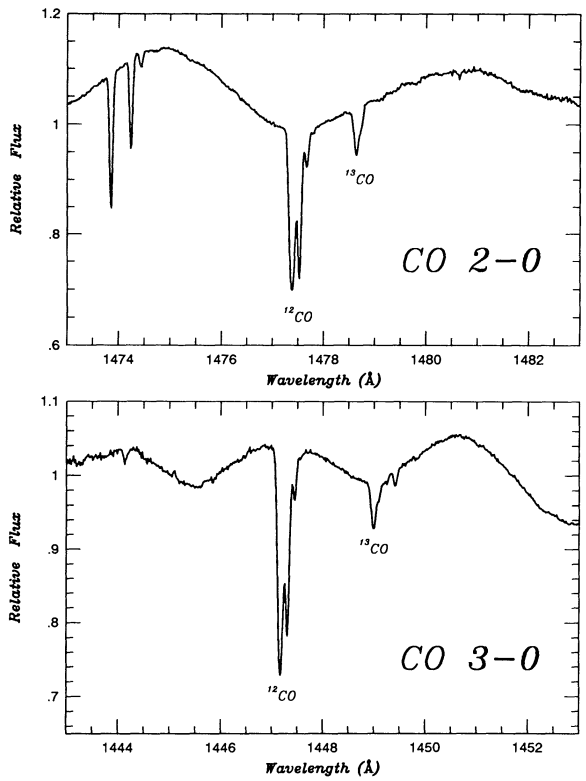

FIG. 1.—1465 Å GHRS G160M spectrum shows the ^{12}CO and ^{13}CO A–X 2–0 (*top*) and 3–0 (*bottom*).

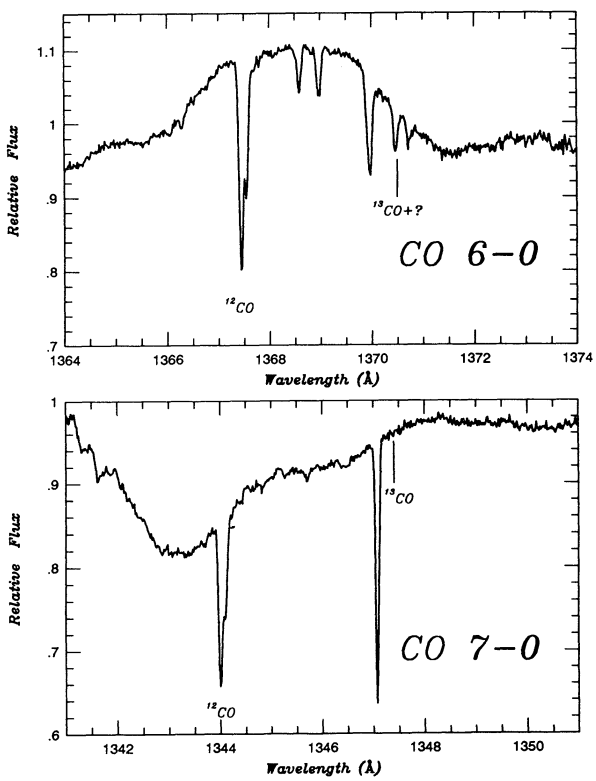

FIG. 2.—1355 Å GHRS G160M spectrum shows the ^{12}CO A–X 6–0 (*top*) and 7–0 (*bottom*) bands. Positions of the undetected ^{13}CO bands are shown.

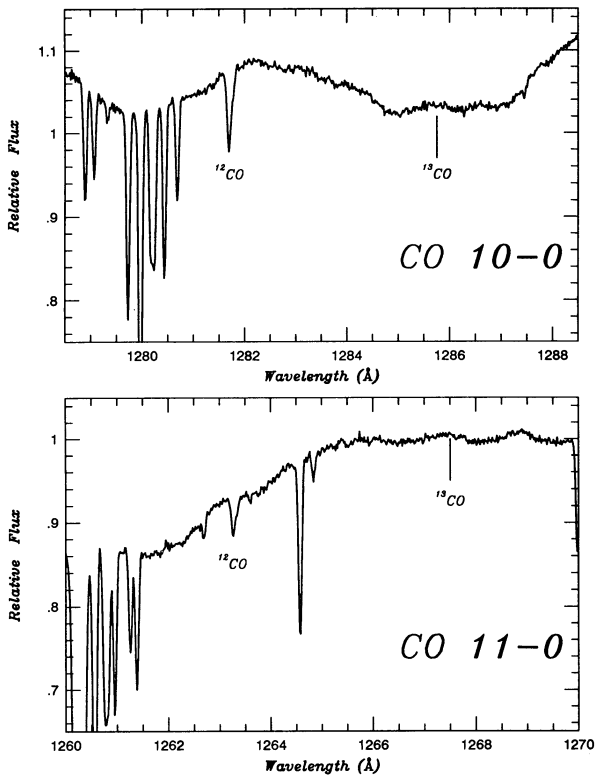

FIG. 3.—1273 Å GHRS G160M spectrum shows the ^{12}CO A–X 10–0 (*top*) and 11–0 (*bottom*) bands. Positions of the undetected ^{13}CO bands are shown.

sure set in which the 1280 Å complex falls near pixel 1200 (of 2000 in quarter-stepped spectra) would be shifted by several Å in a second set, to pixel position 1440 that corresponded to 1285 Å, a region of clean continuum, in the first set. In this way it is possible to cleanly separate any features that arise from the photocathode granularity and stellar spectra.

The problem of separating spectral features arising from quantum efficiency glitches on the photocathode and intrinsic stellar features can be cast in the same tomographic formalism (Bagnuolo & Gies 1991) used to separate composite spectra of binary stars, in which the individual spectral are offset from each other in successive exposures as a result of radial velocity differences. The response at any pixel position i and exposure l can be represented as

$$d_{i,l} = s_{i+os_l} g_{i+og_l} p_i \,, \tag{1}$$

where d represents the data as observed, s represents the intrinsic stellar spectrum, g represents the photocathode response, and p is the pixel sensitivity. The primary offsets, os_l, between the $l = 1$, M spectra result from specified carrousel motions either as part of an FP-SPLIT, or as slightly different central wavelengths as specified in Table 1. Each observed spectrum is 2000 pixels long. The maximum offset of 632 pixels between the 1461 and 1471 Å exposure allow construction of a single stellar spectrum 2,632 pixels long with complete redundancy of all exposures from 1453 to 1479 Å. The granularity vector is 2000 pixels (plus the largest magnitude of $og_l \sim 4$ pixels for this data). The 1465 Å group of spectra involves six basic settings each with four FP-SPLIT subexposures at unit (about 20 pixels) carousel offsets for a total of 24 independent carousel settings. (Each is also repeated 3 times, but no additional offsets are involved.) There are therefore 24 × 2000 observations to constrain a solution for 2632 + 2004 unknown quantities in the independent stellar and granularity vectors. Equation (1) may be cast into the form of Bagnuolo & Gies (1991) by taking the logarithm:

$$dl_{i,l} = sl_{i+os_l} + gl_{i+og_l} + pl_i \,, \tag{2}$$

where for example $dl = \ln(d)$. For a perfectly stable instrument the granularity and pixel responses would be inseparable with og_l equal to zero for all exposures. However, the real instrument experiences minor deflection errors (mainly a result of imperfect shielding from the Earth's magnetic field) that can cause points on the photocathode to have offsets of a few pixels. In data acquired in default mode with COMB = 4 and 4 pixel substepping, a single diode with response not equal to that assumed in calibration reductions will generate a flat-topped signal 16 pixels wide. We found evidence of three diodes with slightly anomalous response and fixed their sensitivity value before initiating an iterative solution for the stellar and granularity vectors. (Routine calibrations correct for variations of diode response. As the instrument ages some diodes experience response changes that are addressed by threshold adjustments for instrument operation and corresponding changes to the ground calibration sensitivity vector. For high precision work it should not be assumed that all routine calibrations are performed without error.)

The equations to be iterated for corrections to sl and gl in equation (2) are

$$gd_i = \frac{\delta \sum_{l=1}^{M} wg_{i+os_l-og_l} wm_l \times (dl_{i-og_l,l} - gl_i - sl_{i+os_l-og_l} - pl_{j-og_l})}{\sum_{l=1}^{M} wg^2_{i+os_l-og_l} wm_l^2} \tag{3}$$

$$sd_j = \frac{\delta \sum_{l=1}^{M} ws_{j+og_l-os_l} wm_l \times (dl_{j-os_l,l} - sl_j - gl_{j+og_l-os_l} - pl_{j-os_l})}{\sum_{l=1}^{M} ws^2_{i+og_l-os_l} wm_l^2} \,, \tag{4}$$

where wm_l are global weights on each of the individual spectra, nominally just $1/\sigma^2$ as indicated by Poisson statistics. The damping factor δ as discussed by Bagnuolo & Gies (1991) has generally been set at 0.8 for these analyses. The wg_i are set to unity, except for a few domains where high stellar lines densities yield poor constraints on photocathode granularity—in this case the wg_i are set to zero. The ws_j are set to one everywhere except for any domains where large deviations occur for the granularity of pixel responses. The indicated sums are performed for all indices remaining within realized bounds for all terms.

The solution is reached by:

1. Estimating the initial offsets, os_l, via inspection and cross correlation between observed spectra (og_l assumed equal to zero to start).

2. Forming an initial guess for the full stellar (mean of shifted spectra) and granularity (median of unshifted spectra) vectors and all offsets.

3. Evaluating equations (3) and (4) and adding in the updates, $sl_j = sl_j + sd_j$ ($j = 1$, 2632), $gl_i = gl_i + gd_i$ ($i = 1$, 2004). (Range of indices will be specific to each case.)

4. Forming current real space solutions for the stellar and granularity vectors separately and resetting the offsets, os_l and og_l, for all spectra via cross correlation. (Fractional pixel shifts are applied by adjusting the dl_i using Fourier transform shifts.

This step gave only a marginal gain of ~1% on S/N attained and ~2% on final resolving power.)

5. Iterating steps (3) and (4) until convergence is indicated by vanishingly small updates. (In practice we performed step [4] only every 5th iteration and obtained convergence in about 50 iterations.)

Before starting the tomographic solution all spectra were normalized to a continuum level of unity using IRAF tasks. Use of logarithms quite naturally imposes a positivity constraint. To avoid complementary mean offsets arising in the stellar and granularity vectors, the granularity vector is normalized to a mean of unity after each iteration. Correct indexing and rational selection of the ws_j and wg_i such that a given range of pixels never contributes to either the granularity or stellar spectra solutions provides protection against rare occurrences of time variable diode response, or excess noise from a single diode.

A final flat-fielded, but not continuum normalized, stellar spectrum is formed by averaging the several individual spectra together using the wm_l and ws_j weights and after dividing out the granularity and pixel sensitivity vectors. All further analyses in this paper make use of these spectra. A formal signal-to-noise (S/N) ratio was evaluated for all solutions using first pixel differences in a several hundred pixel clear region in the continuum flattened solution:

$$\mathrm{S/N} = \left[2N_{px} \Big/ \sum_{j=1}^{N_{px}} (s_{j+1} - s_j)^2 \right]^{1/2} . \quad (5)$$

This equation returns S/N equal to 100 for analysis of a Poisson distribution of mean equal to 10,000.) Evaluated in this way the solutions for the 1465, 1355, and 1273 Å sets show S/N of 902.8, 340.4, and 395.0, respectively; values that are within 5%–10% of the Poisson limit. (The counts per pixel listed in Table 1 are averages over the full spectrum. The S/N for the 1273 Å case is evaluated in a region of spectrum with counts some 10% above the mean which accounts for a S/N higher than allowed based on the Table 1 entries. The S/N domain for the other two regions are well represented by these entries.)

The continuum flattened solution, s_j, is in a convenient form for application of deconvolution. GHRS spectra acquired with the SSA may be deconvolved for resolution gains of ~50%–80% (Gilliland et al. 1992) using the Jansson (1984) technique with some compensating degradation of S/N characteristics. The analysis by Federman et al. (1993) of atomic features are based on the deconvolved spectra.

Standard wavelengths were corrected by the amount necessary to yield correct solutions for the Pt-Ne line positions (Reader et al. 1989) in the WAVECALs shown in Table 2. Typical errors on the standard calibration product were a zero point offset of about 0.1 Å and a dispersion error of 0.01 Å over the 36 Å spectra. Wavelengths for the spectra in Table 1 were corrected ($\Delta\lambda = a0 + b0 \times$ pixel no.) by linear interpolation in the Table 2 offsets. The six spectra at 1465 Å yield an internal standard deviation of 0.026 Å in final zero-point offsets; this is about one-third of a diode and is consistent with general precision expectations. The internal error on the mean wavelength for the 1465 Å set should be ~0.01 Å. The velocity of interstellar features in Zeta Ophiuchi are well-known from previous work. A comparison of wavelengths for easily measured features in the three wavelengths ranges shows that the GHRS-based values are too small by 0.047 ± 0.005 Å (about two-thirds of a diode) or a radial velocity error of about 10 km s^{-1}. The wavelengths used in this study have been adjusted to correct for this apparent error in the GHRS absolute wavelength scale.

TABLE 2

WAVELENGTH CALIBRATION OBSERVATIONS

λ (Å)	Rootname	UT	a0 (Å)[a]	b0 (Å pixel^{-1})
1520.0.....	z0x20107	112.863	0.093	−1.15E-5
1520.0.....	z0x2010a	112.939	0.100	−9.38E-6
1520.0.....	z0x2010d	113.068	0.108	−2.66E-6
1520.0.....	z0x2010g	113.187	0.113	−3.78E-6
1520.0.....	z0x2010l	113.256	0.120	−5.07E-6

[a] Columns have same meaning as for Table 1 except a0 and b0 are derived constant and linear terms required to correct standard wavelength solutions to the known position of Pt–Ne lines. These were all system generated WAVECAL/SPYBALS taken about once per orbit using the Pt–Ne lamp observed for 4.8 s through aperture SC2.

The instrumental profile has been determined from atomic lines, independently of the bands. This has eliminated the need to fit it as a parameter in the synthetic spectra, see § 3.4. The averaging of 24 Gaussian-fitted atomic lines of the narrowest width reveals an instrumental FWHM of $\Delta\lambda = 0.0731 \pm 0.0030$ Å. The exclusion of nine atomic lines, all with FWHM greater than $\Delta\lambda$ by more than 3 σ, has prevented any possible contamination by unresolved blends. Hence, we have R at 1465 Å = 20,000 ± 800 (15.0 ± 0.6 km s^{-1}), R at 1355 Å = 18,500 ± 800 (16.2 ± 0.7 km s^{-1}), and R at 1273 Å = 17,400 ± 700 (17.2 ± 0.7 km s^{-1}). The atomic lines are expected to have an intrinsic width much less than the instrumental width and no correction has been made for the intrinsic width. These determinations of R are from the fully reduced but not deconvolved spectra.

3. ANALYSIS

3.1. *The* CO *Band Profiles*

Interstellar lines seen in spectra of ζ Oph must be measured with respect to an undulating stellar continuum arising from the blending of photospheric lines of the rapidly rotating O9.5 V star. These undulations and the imposed sharp interstellar lines are clearly seen in Figures 1 to 3. As the first step in the analysis of the CO bands, the local continuum around the bands was defined and the spectrum rectified. We represented the local continuum by a low-order polynomial, often a linear relation was deemed to be adequate over a short interval about a CO band.

In our analysis we consider both the equivalent widths and the profiles of the CO bands. An equivalent width integrated across a band includes lines from the R-branch bandhead at about $R(3)$ at the short wavelength limit to the $P(3)$ line at the long wavelength limit. The $P(3)$ line is detectable only for the 2–0 and 3–0 ^{12}CO bands. Table 3 gives the measured equivalent widths from our spectra together with published measurements for some other bands. At the resolution provided by G160M with the SSA, the structure of the strongest bands consists of a broad absorption comprising the $R(0)$, $R(1)$, and $R(2)$ lines which is flanked on the long-wavelength side by a weaker, sharper, and partially resolved blend of the $Q(1)$ and $Q(2)$ lines. The P(2) line is a well resolved line to the long wavelength side of the $Q(1)$ and $Q(2)$ lines. The $P(3)$ line is resolved from other lines. The R and Q branches of the weakest bands are unresolved but the observed feature is obviously

TABLE 3

EQUIVALENT WIDTHS

BAND	W_λ (mÅ) This Paper	Paper I	WPJ[a]
$^{12}C^{16}O$:			
2–0.....	74.4 ± 1.2	...	(74 ± 7)
3–0.....	70.4 ± 1.1	...	(67 ± 6)
4–0.....	...	...	53.9 ± 7.1
5–0.....	...	48.8 ± 1.2	51.5 ± 5.6
6–0.....	42.5 ± 1.3	44.2 ± 1.8	44.0 ± 3.1
7–0.....	33.9 ± 1.6	...	30.2 ± 2.2
8–0.....	...	...	24.6 ± 1.3
9–0.....	...	...	15.7 ± 1.2
10–0.....	10.2 ± 0.9	...	9.3 ± 0.8
11–0.....	5.4 ± 0.7	...	6.9 ± 0.8
12–0.....	...	...	2.9 ± 0.4
$^{13}C^{16}O$:			
2–0.....	11.9 ± 0.6[b]	...	(24.7)
3–0.....	10.3 ± 0.8[b]	...	...
4–0.....	...	...	6.3 ± 2.1
5–0.....	...	3.6 ± 0.3	(9.7 ± 4.2)
6–0.....	[c]	<1.8	5.9 ± 0.7[d]
7–0.....	<1.0	...	...
$^{12}C^{17}O$			
2–0.....	<0.3	...	...
3–0.....	<0.3	...	...

[a] WPJ ≡ Wannier et al. 1982. Values in parentheses are from *IUE* spectra.

[b] Includes a small contribution from the $^{12}C^{18}O$ band (see text).

[c] See text.

[d] Includes the contributions of two unidentified lines.

asymmetric. The rotational structure is illustrated by Figure 4 where we show the 6–0 ^{12}CO band as observed with ECH-A and G160M.

The 2–0 and 3–0 $^{13}C^{16}O$ bands are overlapped by their respective $^{12}C^{18}O$ band such that the small contribution of the latter band must be assessed using synthetic spectra. For several bands, an upper limit is all that can be given for the equivalent width. The 7–0 ^{13}CO band is quite unblended. In Figure 5 we show the region of the 7–0 band after linear rectification to the local continuum. A local continuum is interpolated across the Cl I line on the short wavelength side of the 7–0 band. It is apparent that the local continuum is essentially linear for about ±0.2 to 0.3 Å around the 7–0 band and, with

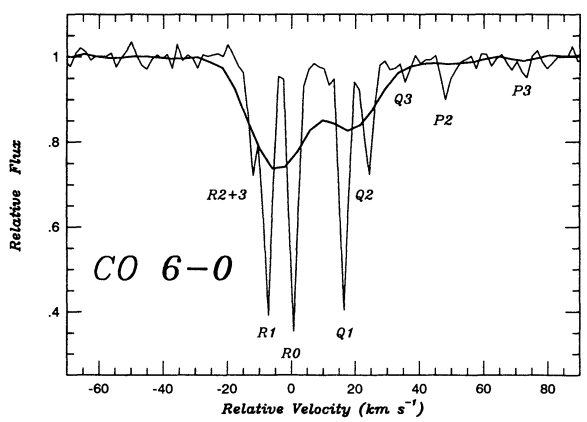

FIG. 4.—Profiles of the ^{12}CO A–X 6–0 band observed with ECH-A (*thin line*) and G160M (*thick line*). Rotational lines from levels 0 to 3 are indicated. While the ECH-A spectrum has a resolution 5 times higher than that of the G160M spectrum, the latter has a S/N ratio 5 times larger than the former.

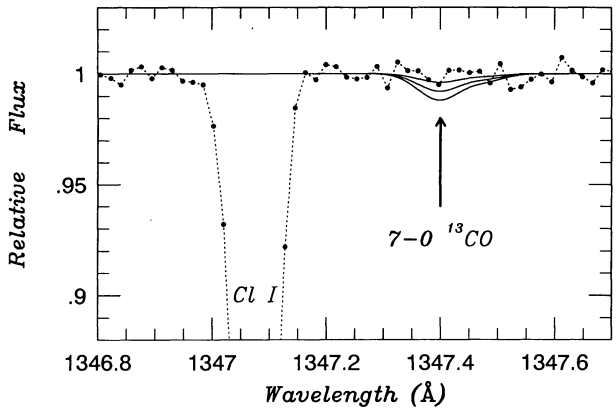

FIG. 5.—1355 Å spectrum covers the expected position of the 7–0 ^{13}CO band. A linearly-rectified local continuum is shown together with predicted profiles for the 7–0 band for W_λ = 0.5, 0.9, and 1.4 mÅ. The interstellar line at 1347.08 Å is due to Cl I.

the obvious exception of the Cl I line, there is no interstellar feature in this interval.

Synthetic ^{13}CO profiles corresponding to equivalent widths of 0.5, 0.9, and 1.4 mÅ are shown superposed on the local continuum. By inspection of Figure 5 a band stronger than 1.0 mÅ is excluded by our spectra. Consideration of the S/N ratio of the spectrum and the width of the band gives a 3 σ limit $W_\lambda < 0.6$ mÅ—see Jenkins et al. (1973) or Cayrel (1988) for the relevant formulae. Thus, our limit $W_\lambda < 1$ mÅ is likely to be a firm upper limit. The $^{12}C^{17}O$ bands which are not detected here lie between the $^{12}C^{16}O$ and $^{13}C^{16}O$ bands. Upper limits are given in Table 3 for the 2–0 and 3–0 $^{12}C^{17}O$ bands' equivalent widths. Comparable limits for the other bands are not given but necessarily provide less stringent limits on the $^{12}C^{17}O$ column density. All rest wavelengths were calculated as described in Paper I.

The calculated wavelengths, as checked against then available measurements, were expected to suffice for reliable identification of even weak bands unless the upper levels are perturbed. Now, recent laboratory measurements of the wavelengths of the 6–0 ^{13}CO lines (Haridass & Huber 1994) show the lowest rotational levels of the upper state to be perturbed; the measured wavelengths differ somewhat from our predicted values. The measured $R(0)$ line, for example, is now coincident with a previously unidentified line (Cardelli et al. 1991; Sheffer et al. 1992) about 15 km s^{-1} from our predicted position, and the line attributed by Sheffer et al. to the $R(0)$ line is possibly the $Q(1)$ line. (A second unidentified line at 1370.61 Å remains unidentified.) The combined equivalent width of the 6–0 ^{13}CO lines as now identified exceeds that of the 5–0 ^{13}CO band even though the unperturbed f-value of the 5–0 band exceeds that of the 6–0 band. Then, the new equivalent width places the 6–0 band well above the weak-line portion of the ^{13}CO curve of growth as defined by the 5–0 and 7–0 bands for which the laboratory and predicted wavelengths are in excellent agreement. We suppose that the interstellar line now coincident with the ^{13}CO $R(0)$ line is either primarily due to a transition other than CO, or the f-value is increased thanks to the perturbation of the upper state. In what follows we neglect the 6–0 ^{13}CO band.

3.2. *Band Oscillator Strengths, $f(v', v'')$*

There is an extensive literature on the radiative properties of the A–X system. The most recent measurements of the band

oscillator strengths [$f(v', v'')$-values] are by Eidelsberg et al. (1992) and Chan, Cooper, & Brion (1993) who both review previously published experimental and theoretical results. We restrict our comments to the four experiments that have provided the most accurate results for the $f(v', v'')$-values. We assume, as discussed in Paper I, that the measurements for $^{12}C^{16}O$ are applicable to other isotopic flavors of CO. Since our conclusions about the interstellar clouds depend on the accuracy of the adopted $f(v', v'')$-values, we comment briefly on the different kinds of experiments whose results are summarized in Table 4.

Eidelsberg et al. (1992) measured the integrated absorption cross sections using a synchrotron light source and a spectrometer at a resolution of 0.15 Å. An accuracy of ±10% was claimed for individual $f(v', v'')$-values. This accuracy appears not to contain a significant component common to all bands (i.e., a scale error) and, hence, a ratio of $f(v', v'')$-values is seemingly not more accurate than individual $f(v', v'')$-values.

Lassettre & Skerbele (1971) and Meyer & Lassettre (1971) provide $f(v', v'')$-values from inelastic electron scattering cross sections. The quoted accuracy is about 5% for all bands except for the 2–0 (also 1–0 and 0–0) for which 10% is claimed. No reduction of these uncertainties seems likely for ratios of $f(v', v'')$-values. The first study of isotopic fractionation of CO toward ζ Oph by WPJ used $f(v', v'')$-values from Lassettre & Skerbele (1971), but excluded those measurements obtained with low-energy electrons. WPJ's adopted values, which are listed in Table 4, differ slightly from the values attributed by Eidelsberg et al. to Lassettre and his colleagues. WPJ's values, which apparently had Lassettre's blessing, are quoted with three significant figures. An implication is that WPJ's values are accurate to better than the 5% referred to above. Unfortunately, WPJ omitted to discuss the likely errors in their adopted $f(v', v'')$-values; we presume that 5% (10% for 2–0) is the appropriate estimate. For all but the 11–0 band WPJ's values coincide with the values attributed by Eidelsberg et al. to the electron scattering experiments. WPJ quote $f(11, 0) = 0.203$ but Eidelsberg et al. give $f(11, 0) = 0.25 \pm 0.01$.

Chan et al. (1993) also report on inelastic electron scattering experiments. An accuracy of 5% is claimed for the $f(v', v'')$-values except, perhaps, for the weakest bands or $v' \gtrsim 9$. For $v' \leq 8$, Chan et al.'s results are 4% to 8% smaller than the values reported by Lassettre & Skerbele (1971); the mean difference from the eight bands is 6.0 ± 1.6%. The $f(v', v'')$-values for the 1–0 and 2–0 bands by Eidelsberg et al. attributed to Lassettre and colleagues are 40% and 12% larger than Chan et al.'s values.

Measurements of the radiative lifetimes ($\tau_{v'}$) of vibration levels in the $A^1\Pi$ state may be converted to $f(v', v'')$- values. Since the decay of a level v' is determined by transitions to several vibrational levels (v'') in $X^1\Sigma^+$, it is necessary in the conversion of a set of lifetimes to f-values to know (or infer) a form for the variation of the electronic transition moment [$R_e(r)$] with internuclear separation (r). Field et al. (1983), whose measurements of $\tau_{v'}$ are the most extensive ($v' = 0$ to 7) and most precise of published values, adopted a linear form for $R_e(r)$. De Leon (1988, 1989) extended Field et al.'s $R_e(r)$ to larger internuclear separations with his measurements of the relative intensities of laser-induced emissions from $A^1\Pi$ to high vibrational levels (v'') of $X^1\Sigma^+$. Eidelsberg et al. (1992), who computed $f(v', v'')$-values from Field et al.'s lifetimes and De Leon's quadratic form for $R_e(r)$, show that De Leon's $R_e(r)$ is in good agreement with their own $f(v', v'')$-values. By contrast, Chan et al.'s (1993) $f(v', v'')$-values lead to flatter variation of $R_e(r)$ with r; this simply reflects the fact that Chan et al.'s $f(v', v'')$-values for $v' \geq 9$ are smaller than those from the other experiments (see Table 4). There is some theoretical support (see Eidelsberg et al. 1992; Chan et al. 1993) for the flatter $R_e(r)$. We also give in Table 4, the $f(v', v'')$-values adopted by WPJ and in Paper I.

3.3. *The* CO *Curves of Growth*

The $^{12}CO/^{13}CO$ ratio was derived previously by superposing the ^{13}CO empirical curve of growth on its ^{12}CO counterpart. In this section, we follow this precedent and discuss the curves of growth for the four different sets of experimental $f(v', v'')$-values in Table 4. Since the ^{13}CO bands are weak ($W_\lambda \lesssim 12$ mÅ), we here consider only the weak bands of the ^{12}CO system. The rotational structure of the CO bands varies slightly with v' and isotopic species. Equivalent widths estimated from our synthetic spectra (see below) show that ^{12}CO and ^{13}CO curves of growth for these bands with $W_\lambda \lesssim$ 12 mÅ differ by a negligible extent when identical physical conditions are adopted for the two molecules.

TABLE 4

$f(v', v'')$-VALUES FOR THE CO $A^1\Pi$–$X^1\Sigma^+$ SYSTEM

	$10^3 f v'v''$ EXPERIMENTAL[a]				$10^3 f v'v''$ PREVIOUSLY ADOPTED[b]	
v'–0	ERBT	LS+ML	DeL	Chan	WPJ	Paper I
1–0.....	33.7 ± 3.4	49 ± 4	33 ± 4	35.1 ± 1.8	37.9	34.2
2–0.....	42.4 ± 4.2	45 ± 5	40 ± 5	40.2 ± 2.0	42.9	41.1
3–0.....	37.7 ± 3.7	36 ± 2	35 ± 4	34.7 ± 1.7	36.4	36.0
4–0.....	25.8 ± 2.6	25 ± 1	26 ± 3	24.2 ± 1.2	25.1	25.7
5–0.....	16.3 ± 1.6	15.5 ± 0.7	16 ± 2	14.5 ± 0.7	15.4	16.1
6–0.....	10.4 ± 1.0	8.5 ± 0.4	9.0 ± 1	8.05 ± 0.40	8.34	9.09
7–0.....	5.6 ± 0.6	4.4 ± 0.2	5.0 ± 0.4	4.14 ± 0.02	4.28	4.78
8–0.....	2.9 ± 0.3	2.2 ± 0.1	2.6 ± 0.3	2.02 ± 0.10	2.11	2.38
9–0.....	1.4 ± 0.2	1.08 ± 0.05	1.16 ± 0.06	0.95 ± 0.09	0.993	1.14
10–0.....	0.65 ± 0.07	0.50 ± 0.03	0.60 ± 0.06	0.41 ± 0.04	0.463	0.530
11–0.....	0.28 ± 0.03	0.25 ± 0.01	0.28 ± 0.02	0.18 ± 0.02	0.203	0.241
12–0.....	0.13 ± 0.02	0.10 ± 0.005	0.13 ± 0.01	0.09 ± 0.01	0.088	0.108

[a] ERBT ≡ Eidelsberg et al. 1992; LS+ML ≡ Lassettre & Skerbele 1971 and Meyer & Lassettre 1971; DeL ≡ De Leon 1988, 1989; Chan ≡ Chan et al. 1993.

[b] WPJ ≡ Wannier et al. 1982; Paper I ≡ Sheffer et al. 1992.

The slopes of the curves of growth at $W_\lambda \lesssim 12$ mÅ are dependent on the accuracy of the measured equivalent widths. Except for the (uncertain) measurement of the 4–0 band (from WPJ), the $^{13}C^{16}O$ W_λ's are based on GHRS spectra from this paper or Paper I; the 5–0 measurement is based on a fairly high S/N (=170) echelle spectrum taken through the LSA so that the effective spectral resolution was about twice that of our G160M spectra. The estimated uncertainty of the W_λ of the 2–0 band is based on the assumption that the local continuum varies smoothly across the line. Inspection of Figure 1 shows, however, that the stellar spectrum is rippled on the long-wavelength side of the band. This structure is attributable to the granularity of the digicon's photocathode. The rippling appears to decrease in amplitude as the wavelength approaches that of the 2–0 band; there is no evidence of rippling on the short-wavelength side of the band. If a depression like that evident at 1479 Å were present at the location of the 2–0 band, the W_λ would be overestimated by about 1.3 mÅ. The 3–0 band falls near the center of a weak stellar line so that definition of the local continuum is less certain than for other bands; we estimate this uncertainty may amount to about ± 1.0 mÅ. An unidentified line falls at 1449.43 Å with a suspicion that a weaker line is present at 1449.25 Å. Since such lines are rare in these spectra we presume the juxtaposition of these lines and the ^{13}CO band is a chance occurrence and that there is only a small probability that an unidentified line lies undetected under the ^{13}CO band. The slope attributed to the ^{13}CO curve of growth is particularly dependent on the upper limit for the 7–0 band. This band is quite unblended, and we estimate $W_\lambda \leq 1$ mÅ (see § 3.1).

The wavelength shift between the $^{12}C^{18}O$ and $^{13}C^{16}O$ v'–0 bands is so small that our W_λ's for the 2–0 and 3–0 bands include the contribution of both molecules. Comparison of observed and synthetic band profiles (see below) allows for a partial resolution of the very weak $^{12}C^{18}O$ contribution to the weak $^{13}C^{16}O$ band, but the $^{12}C^{18}O$ contribution to the W_λ-values of the $^{13}C^{16}O$ bands should be recognized in discussion of the curves of growth. The larger isotopic wavelength shifts for the 5–0, 6–0, and 7–0 bands place the $^{12}C^{18}O$ lines outside the wavelength limits defining the equivalent widths of the $^{13}C^{16}O$ bands.

The ^{12}CO bands 12–0, 11–0, and 10–0 span the W_λ range of the ^{13}CO bands and the slightly stronger 9–0 and 8–0 bands assist in the definition of the curve of growth. Our spectra (Fig. 3) provide accurate W_λ's for the 11–0 and 10–0 bands. WPJ's W_λ measurements off *Copernicus* spectra are adopted for the 12–0, 9–0, and 8–0 bands. Table 3 shows that WPJ's W_λ from *Copernicus* spectra are in good agreement with measurements reported here and in Paper I off GHRS spectra. Therefore, we accept the 12–0 band's W_λ given by WPJ.

Definition of the curves of growth is, of course, dependent on the choice of the $f(v', v'')$-values. The ^{13}CO curve of growth is defined by the bands $v' = 7$ to 2 and the ^{12}CO curve of growth for bands of the same W_λ as the ^{13}CO bands depends on $v' = 12$ to 8. The most effective demonstration of the dependence of the isotopic ratio $^{12}CO/^{13}CO$ on the $f(v', v'')$-values is to discuss the ^{12}CO and ^{13}CO curves of growth corresponding to a chosen set of $f(v', v'')$-values.

Eidelsberg et al.'s (1992) $f(v', v'')$-values lead to a ^{13}CO curve of growth (Fig. 6) with a slope steeper than that of the ^{12}CO curve of growth and even steeper than that expected in the linear or weak-line limit. In Figure 6, we show the ^{12}CO curve of growth based on a fit to all the ^{12}CO bands. This fits shows

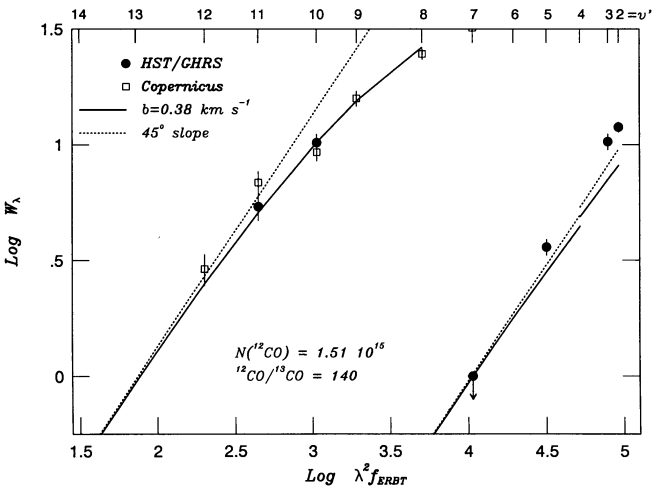

FIG. 6.—Curves of growth for the 8–0 to 12–0 ^{12}CO and the 2–0 to 7–0 ^{13}CO bands based on Eidelsberg et al.'s (1992) $f(v', v'')$-values. The break in the ^{13}CO curves between $v' = 3$ and 4 occurs because the W_λ predictions for the 2–0 and 3–0 ^{13}CO bands include a $^{12}C^{18}O$ contribution with $^{12}C^{16}O/^{12}C^{18}O = 1550$.

that even the 11–0 and 12–0 bands are slightly saturated. The isotopic ratios summarized in Table 5 are based on empirical curves of growth (smooth curves through the data points). We later give results based on the "true" curves of growth. We assume that the maximum possible slope for the linear curve of growth is 45°, i.e., $W_\lambda \propto f(v', v'')\lambda^2$. Although we suggest below a reason why the observed ^{12}CO and ^{13}CO curves of growth may have different slopes over the equivalent width range covered by the weakest bands observed by us, we cannot imagine physical conditions under which the slope can exceed 45° for weak lines formed in interstellar diffuse clouds. We suppose that the steeper than expected slope may in part be due to systematic errors affecting the f-values and/or to contamination of the 2–0 and 3–0 band W_λ's with a $^{12}C^{18}O$ contribution. The $^{12}CO/^{13}CO$ ratio is best set by the 7–0 and 5–0 bands. The lower limit set by the former exceeds the estimate from the 5–0 band (see Table 5). The 5–0 band and the relative $f(v', v'')$-values imply $W_\lambda \sim 1.2$ mÅ for the 7–0 band which is probably at odds with the observed limit (Fig. 5). Adjustment of the ratio $f(5, 0)/f(7, 0)$ within the range suggested by the experimental uncertainties [about $\pm 10\%$ for a $f(v', v'')$] could perhaps reduce the predicted W_λ close to the observed limit. A ratio $^{12}CO/^{13}CO \sim 130$ is a compromise between the 5–0 and 7–0 bands. This limit is what we find by constructing an empirical curve of growth through the ^{12}CO points and translating this curve to pass between the 5–0 and 7–0 ^{13}CO bands.

The 2–0 and 3–0 ^{13}CO bands are expected to lie above the true ^{13}CO curve of growth because these bands are contaminated with contributions from the $^{12}C^{18}O$ bands. The $^{12}C^{16}O/^{12}C^{18}O$ ratio needed to place the adjusted W_λ's of the 2–0 and 3–0 ^{13}CO bands on a ^{13}CO curve of growth are given in Table 5 for four possible empirical curves of growth: linear curves fitted to either the 7–0 or 5–0 ^{13}CO bands, and ^{12}CO-like curves also fitted to either the 7–0 or 5–0 bands. Since the $^{12}C^{18}O$ lines are displaced in wavelength from their counterparts, the profiles of the 2–0 and 3–0 bands betray information on the $^{12}C^{18}O$ column density. In the next section, we find that $^{12}C^{16}O/^{12}C^{18}O \sim 1500$ is suggested by the profiles. Then, three of the four possible curves of growth constructed from

TABLE 5

COLUMN DENSITY AND ISOTOPIC RATIOS

f-VALUES	$N(^{12}CO)^a$ [cm^{-2}]	$^{12}CO/^{13}CO^b$ 7–0	$^{12}CO/^{13}CO^b$ 5–0	$^{12}C^{16}O/^{12}C^{18}O^c$ 7–0 Linear	$^{12}C^{16}O/^{12}C^{18}O^c$ 7–0 ^{12}CO-like	$^{12}C^{16}O/^{12}C^{18}O^c$ 5–0 Linear	$^{12}C^{16}O/^{12}C^{18}O^c$ 5–0 ^{12}CO-like
ERBT	1.6×10^{15}	>150	125	330	240	925	350
LS+ML	2.1×10^{15}	>150	155	1100	440	>1300	420
DeL	1.6×10^{15}	>130	125	415	260	750	350
Chan	2.3×10^{15}	>150	160	1200	640	1500	650

[a] From the 12–0 band and the assumption that it is unsaturated.

[b] From either the 7–0 or the 5–0 ^{13}CO band and the 12–0 ^{12}CO band and the assumption that the three bands are unsaturated.

[c] From the requirement that the adjusted W_λ's of the 2–0 and 3–0 ^{13}CO band fall on the curve of growth fitted to the W_λ of either the 5–0 or the 7–0 ^{13}CO band. The ratio $^{12}C^{16}O/^{12}C^{18}O$ is given for the assumption that the ^{13}CO curve of growth is linear up to at least $W_\lambda = 12$ mÅ and for an alternative assumption that the ^{13}CO and ^{12}CO curves have the same shape.

Eidelsberg et al.'s $f(v', v'')$-values may be dismissed as requiring implausibly high $^{12}C^{16}O/^{12}C^{18}O$ ratios in order to place the 2–0 and 3–0 ^{13}CO bands on the curve. The one (marginally) acceptable case is the linear curve of growth fitted to the 5–0 ^{13}CO band.

The $f(v', v'')$-values based on the electron energy-loss experiments by Lassettre and colleagues (see column "LS+ML" in Table 4) provide a more consistent ^{13}CO curve of growth in that the $^{12}CO/^{13}CO$ ratio from the 5–0 band is consistent with the lower limit from the 7–0 band and the assumption of a linear ^{13}CO curve of growth results in a $^{12}CO^{16}/^{12}C^{18}O$ ratio consistent with that obtained from the profiles of the 2–0 and 3–0 ^{13}CO bands (see Table 5).

De Leon's (1988, 1989) derivation of the electronic transition moment $R_e(r)$ leads to the $f(v', v'')$-values quoted by Eidelsberg et al. (1992) and given in Table 4. This set of $f(v', v'')$-values requires an unacceptably low $^{12}C^{16}O/^{12}C^{18}O$ ratio in order to fit the reduced W_λ of the 2–0 and 3–0 ^{13}CO bands onto a curve of growth fitted to either the 5–0 or 7–0 ^{13}CO bands.

The $f(v', v'')$-values provided by Chan et al. (1993) provide a pleasingly consistent set of curves of growth (Fig. 7). The 5–0 and 7–0 ^{13}CO bands give a consistent $^{12}CO/^{13}CO$ ratio ($\simeq$160). The $^{12}C^{16}O/^{12}C^{18}O$ ratios ($\sim$1000–1500) required to put the adjusted W_λ's of the 2–0 and 3–0 ^{13}CO bands onto a linear curve of growth are roughly consistent with estimates from the profile analyses. Note, however, that a low $^{12}C^{16}O/^{12}C^{18}O$ ratio is implied if the ^{13}CO and ^{12}CO curves of growth have the same shape.

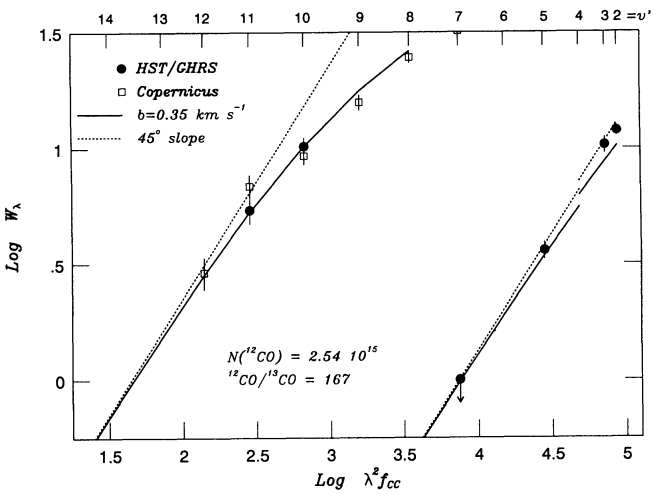

FIG. 7.—Same as Fig. 6, but with band syntheses now based on Chan et al.'s (1993) $f(v', v'')$-values. Note that the agreement with the progression of observed equivalent widths is better than that obtained in Fig. 6.

Of the quartet of experimental $f(v', v'')$-values, the electron scattering experiments of Chan et al. (1993) and Lassettre and colleagues provide the most consistent results: $^{12}CO/^{13}CO \sim 160$ with a strong suggestion that the ^{13}CO curve of growth is linear to at least $W_\lambda \simeq 12$ mÅ in contrast to the ^{12}CO curve of growth. The other pair of experimental results demand a $^{12}C^{16}O/^{12}C^{18}O$ ratio that is not confirmed by the profile analyses but the $^{12}CO/^{13}CO$ ratio is clearly similar to the value of 160 provided from the $f(v', v'')$-values given by the electron scattering experiments. The curves of growth (Figs. 6 and 7) are based on the synthetic spectra discussed below. When the slight saturation of the weakest ^{12}CO bands is considered, the $f(v', v'')$-values from Chan et al. (1993) give $^{12}CO/^{13}CO = 167$ and a column density $N(^{12}CO) = 2.5 \times 10^{15}$ cm^{-2}.

A search for the $^{12}C^{17}O$ 2–0 and 3–0 bands yielded negative results—see Figure 8. The 3 σ limit to the band's equivalent widths are $W_\lambda \lesssim 0.33$ mÅ which correspond to $^{12}C^{16}O/^{12}C^{17}O > 5900$ and 4900 for the 2–0 and 3–0 bands, respectively, when Chan et al.'s $f(v', v'')$-values are adopted.

3.4. *Synthetic Spectra*

The profiles of the CO bands which were not considered in the discussion of the empirical curves of growth, carry information about the physical conditions in the cloud layers containing the CO molecules. Differences in the mean physical conditions of the layers containing ^{12}CO and the ^{13}CO are presumably responsible for the differences between the ^{12}CO and ^{13}CO empirical curves of growth. In this section we explore the range of physical conditions by matching synthetic and observed band profiles.

Molecules such as CO are not contained within a single cloud along the line of sight to ζ Oph. High-resolution absorption spectra of the CN 3874 Å and CH 4300 Å lines show that these molecules are distributed across two clouds (Lambert, Sheffer, & Crane 1990). At a resolution of about 0.5 km s^{-1} the observed CN line was almost fully resolved and shown to comprise two Gaussian components separated by 1.18 km s^{-1}. The ratio of the column densities of the two clouds was $\Phi = 0.30$

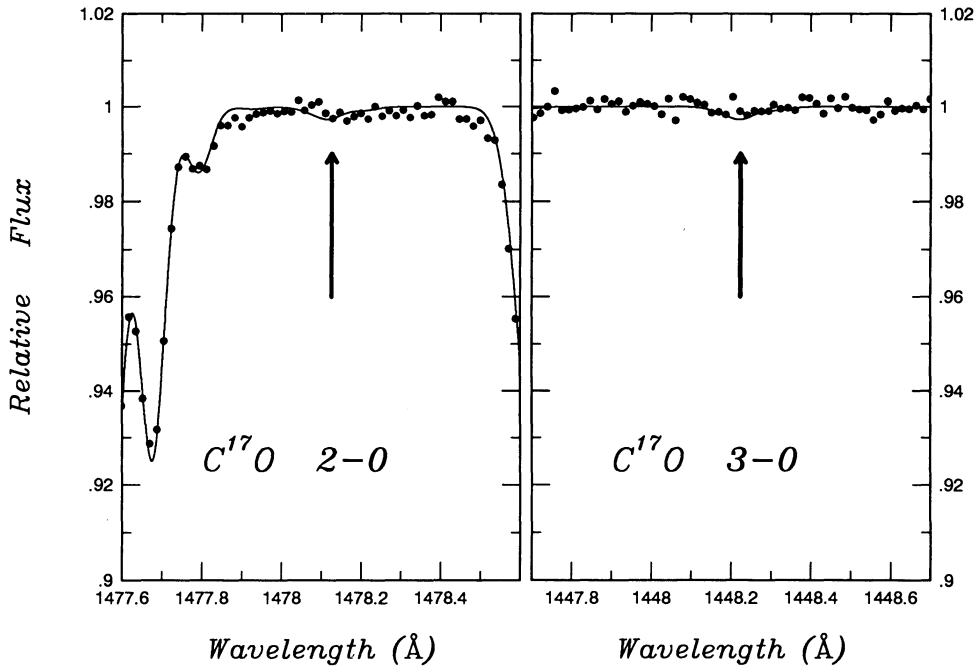

FIG. 8.—1465 Å spectrum showing a linearly rectified local continuum near the $^{12}C^{17}O$ 2–0 (*left*) and 3–0 (*right*) bands. A predicted band profile corresponding to $W_\lambda = 0.33$ mÅ is plotted for both bands, with both $^{12}C^{16}O$ and $^{13}C^{16}O$ bands partially visible towards the boundaries of the 2–0 frame.

with the CN-poor cloud having the higher radial velocity. The CN-rich cloud has a large half-width: $b = 0.59 \pm 0.04$ km s^{-1} but 0.38 ± 0.08 km s^{-1} for the CN-poor cloud. (The FWHM of the line is FWHM $= 2\sqrt{\ln 2}\, b = 1.665b$). Decomposition of the CH profile was more complex because it contains a much broader component from the warm (shocked?) gas that provides the observed CH^+ line at 4232 Å ($b = 2.10$ km s^{-1} for CH^+ and 3.1 km s^{-1} for the CH^+-like component of CH). The CN-like CH components have $b = 0.75$ and 0.44 km s^{-1} for the CN-rich and CN-poor components, respectively. The two clouds have very similar CH column densities ($\Phi \simeq 1$); the CN/CH ratio is roughly 3 to 1 in favor of the lower radial velocity component.

The presence of two clouds cannot be discerned directly from the GHRS spectra; even ECH-A provides a resolution no better than about 3 km s^{-1}. Fortunately, observations of the CO $J = 1$–0 and 2–1 emission lines at millimeter wavelengths (e.g., Le Bourlot, Gerin, & Perault 1989) show the presence of two clouds in the vicinity of ζ Oph. Observations taken directly toward the star with a 23″ beam show two Gaussian components with a velocity separation of 1.18 ± 0.02 km s^{-1}, precisely the separation of the CN components. The widths correspond to $b = 0.36 \pm 0.01$ and 0.52 ± 0.02 km s^{-1} for the CN-rich and CN-poor clouds, respectively. The CN-rich cloud is also the CO-rich cloud: the ratio was $\Phi = 0.47$ for CO. Similar results were obtained recently by Wilson et al. (1992) from the $J = 1$–0 line observed towards ζ Oph with a 45″ beam: $b = 0.47 \pm 0.02$ and 0.66 ± 0.06 km s^{-1} with $\Phi = 0.72$. Lambert et al. (1990) used the relative widths of the CN and CN-like CH components to infer that the cloud with the majority of the molecules had the higher kinetic temperature: $T = 340 \pm 60$ K versus $T = 80 \pm 60$ K. (The b-values for CO corresponding to these temperatures are 0.45 and 0.22 km s^{-1}, respectively.) The turbulent velocity was estimated to be about 0.5 km s^{-1} in both clouds. This decomposition of the line widths was based on the implicit assumption that CN and CH are collocated in the clouds. The locations of the two clouds along the line of sight are unknown.

The gas containing the CH^+ ions ($b = 2.1$ km s^{-1}) and the CH^+-like fraction of the CH molecules ($b = 3.1$ km s^{-1}) is evidently not contributing to the CN absorption line or to the CO emission or absorption lines. If thermal velocities dominate these large b-values, one expects the comparable CO line to have a width (FWHM) of 2.4 to 3.5 km s^{-1}. If turbulence or streaming motions, as predicted behind a shock, contribute to the FWHMs of the CH^+ of the CH^+-like CH lines, the comparable CO line will have a FWHM more nearly like 3.5 to 5.2 km s^{-1}. In Paper I, we argued that the CO line profiles on the ECH-A spectra did not admit of more than 4% of the total CO column density belonging to the gas containing the CH^+ ions. There is similarly a lack of evidence in the CO $J = 1$–0 and 2–1 emission profiles for CO associated with CH^+ ions.

Our syntheses of the profiles of the ^{12}CO and ^{13}CO bands assume that the line of sight passes through two identical clouds of uniform density, and temperature. We assume that the radial velocities of the clouds differ by 1.18 km s^{-1} which is the value provided by the CO mm emission and the CN absorption lines. We fit synthetic profiles to the six ^{12}CO bands observed here; synthetic profiles are convolved with the instrumental profile (§ 2). In view of the discussion in the preceding section, we suppose that the $f(v', v'')$-values provided by Chan et al. (1993) may give the most reliable results but we also did the complete analysis for the $f(v', v'')$-values reported by Eidelsberg et al. (1992). The parameters adjusted in obtaining a fit include the total column density $N(12)$, the three excitation temperatures $T(J, J-1)$ for $J = 1$, 2, and 3, the ratio of the column density in the "red" to the "blue" cloud Φ, and the turbulent velocity or b-value which is assumed to be identical for the two clouds. The final fits to the six $^{12}C^{16}O$ bands, which are shown in Figure 9, correspond to the set of parameters listed in Table 6; the illustrated differences between the observed and synthetic spectra show the excellence of the fits.

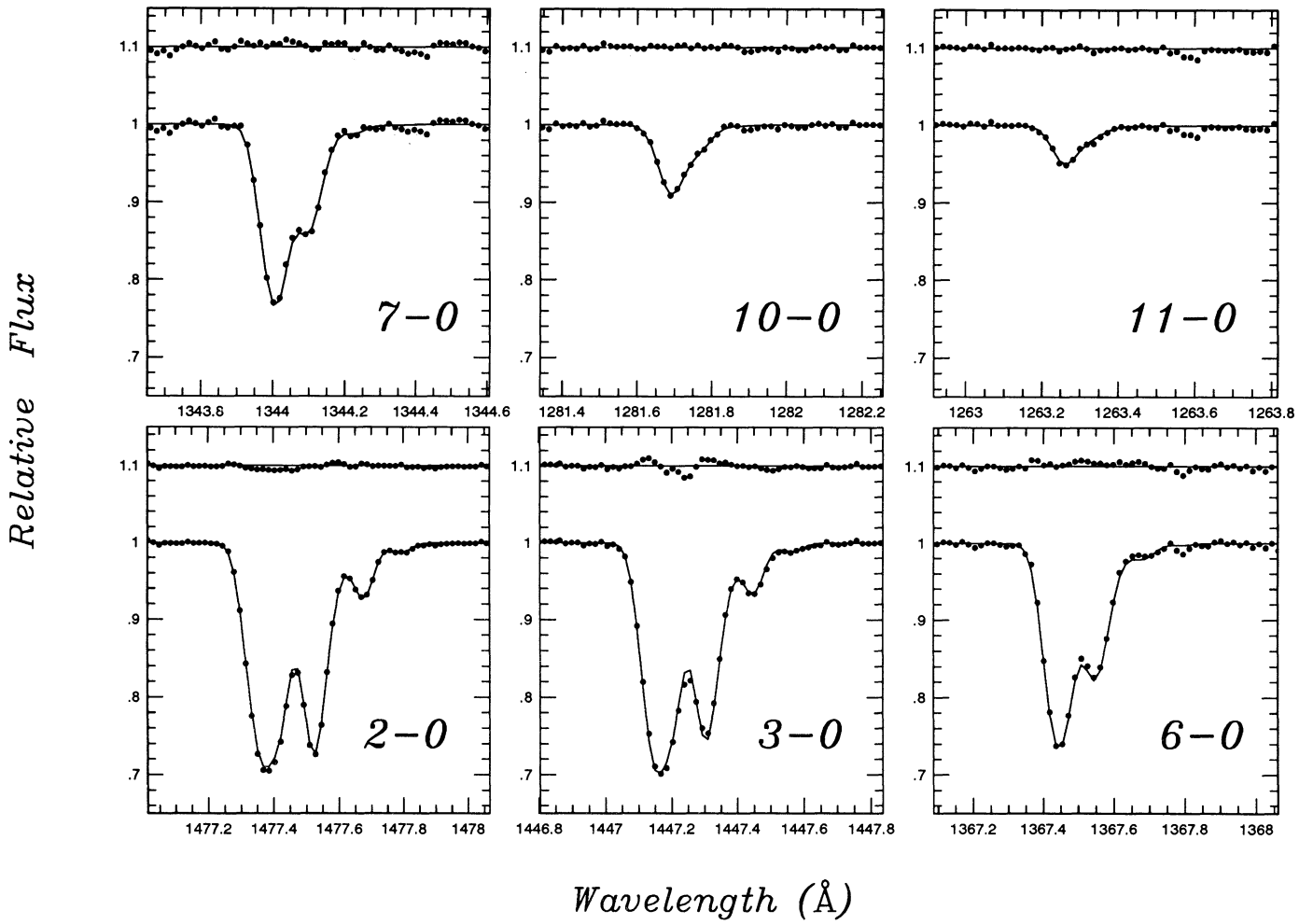

FIG. 9.—Observed and synthesized band profiles for ^{12}CO bands. The synthetic profiles are based on the parameters in Table 6 (see column headed "Chan et al."). In each panel, the residuals following a subtraction of the synthetic profile from the observed spectrum are shown with an arbitrary upward shift by 1.1 continuum units.

The errors assigned to these entries are such that, if a given quantity is changed by the quoted error, the fit to one or more bands is significantly degraded. Certain parameters are correlated; for example, the fraction Φ can be altered by somewhat more than the indicated error if the *b*-value is adjusted to compensate.

The column density $N(12)$ is set by the relatively unsaturated 11–0 and 12–0 bands. The profiles of the 11–0 and 10–0 bands are sensitive to the excitation temperature $T(1, 0)$. The stronger 7–0 and 6–0 bands influence the determination of $T(2, 1)$; the $P(2)$ line is well resolved for these bands. The temperature $T(3, 2)$ is found from the weak $P(3)$ line seen only in the 2–0 and 3–0 bands and the moderately saturated $P(2)$ line of the same bands. The *b*-value's principal influence is on the total equivalent widths of the strongest bands. We have checked that the higher resolution spectra of the 5–0 and 6–0 spectra from Paper I are adequately fit using the parameters given in Table 6. The fraction Φ's influence is primarily on the saturated bands and, hence, estimates of Φ are correlated with the *b*-value and the excitation temperature. No attempt was made in Paper I to determine excitation temperatures for pairs of rotational levels. The mean excitation temperature from the low S/N ECH-A spectra of 4.2 ± 0.3 K is in good agreement with our new results: the mean of $T(1, 0)$ and $T(2, 1)$ is 4.28 K. Our estimate of *b* (assumed to be the same for the two clouds) is in good agreement with Le Bourlot et al.'s (1989) estimate for the stronger cloud (0.35 vs. 0.36 km s^{-1}).

A similar synthesis of the 2–0 and 3–0 ^{13}CO bands was made using Chan et al.'s $f(v', v'')$-values and including a contribution from the $^{12}C^{18}O$ band. Synthetic and observed profiles of these bands are shown in Figure 10. In obtaining these fits,

TABLE 6

PHYSICAL CONDITIONS

PARAMETER	^{12}CO $f(v', v'')$ from Eidelsberg et al.	^{12}CO $f(v', v'')$ from Chan et al.	^{13}CO $f(v', v'')$ from Chan et al.
N (cm^{-2})	$(1.72 \pm 0.11)10^{15}$	$(2.54 \pm 0.16)10^{15}$	$(1.52 \pm 0.10)10^{13}$
$T(1, 0)$ (K)	3.9 ± 0.4	3.4 ± 0.4	4.2 ± 0.4
$T(2, 1)$ (K)	4.6 ± 0.2	4.5 ± 0.2	4.4 ± 0.2
$T(3, 2)$ (K)	6.3 ± 0.5	5.9 ± 0.5	5.9 ± 0.5[a]
Φ	0.36 ± 0.12	0.36 ± 0.1	0.36 ± 0.1[a]
b (km s^{-1})	0.37 ± 0.1	0.35 ± 0.1	0.35 ± 0.1[a]

[a] Values adopted from ^{12}CO.

we considered adjustments to the excitation temperatures. The parameter Φ was kept at 0.36. In light of our conclusion that the ^{13}CO curve of growth is linear for these bands, we increase the b-value to the minimum necessary to ensure a linear curve of growth ($b \simeq 2.0$ km s^{-1}). Inspection of the ^{13}CO–$C^{18}O$ profiles shows that $^{12}C^{16}O/^{12}C^{18}O = 1550 \pm 440$ is a compromise result for the two bands; the optimum fit to the 2–0 band gives $^{12}CO/^{13}CO = 164$ and $C^{16}O/C^{18}O = 1640$ with the 3–0 band providing $^{12}CO/^{13}CO = 171$ and $C^{16}O/C^{18}O = 1460$ for Chan et al.'s $f(v', v'')$-values. As noted above, the local continua to the $^{12}C^{18}O$-side of the 2–0 and 3–0 $^{13}C^{16}O$ bands are subject to uncertainties arising from the granularity of the photocathode (the 2–0 band) and weak interstellar lines (the 3–0 band). These uncertainties probably account for the relatively poor agreement between the $^{12}C^{18}O$ column density estimates from the two bands. Our attempt to fit all the band profiles is tantamount to constructing a theoretical curve of growth. This curve shows that the 12–0 ^{12}CO band is slightly saturated (see Figs. 6 and 7). Recognition of this fact leads to a small increase of the $^{12}CO/^{13}CO$ ratios in Table 5. We note that the observed resolved lines of the $B-X$ 0–0 band at 1150 Å (see Paper I) are well fitted with the physical conditions in Table 6 derived from Chan et al.'s (1993) $f(v', v'')$-values and their f-value for the $B-X$ band: $f(0, 0) = 0.00803$.

4. DISCUSSION

4.1. *Cloud Temperature and Density*

Interpretation of the fractionation implied by the ratio $^{12}CO/^{13}CO \simeq 170$ calls for estimates of the density (n_H) and temperature of the gas (T) containing the CO molecules. In this section, we assemble estimates of n_H and T from various monitors of the clouds' physical conditions.

4.1.1. CO *Excitation Temperatures*

The excitation temperatures of the CO molecule result from the collisional excitation and de-excitation of the rotational levels with radiative excitation by the cosmic microwave background radiation and spontaneous emission also included. These processes are modeled using a large-velocity gradient (LVG) code (Snell 1981). The n_H versus T loci required to reproduce $T(1, 0)$, $T(2, 1)$, and $T(3, 2)$ are shown in Figure 11 (*left*); the two loci for a given temperature correspond to the maximum and minimum temperatures from Table 6 for the ^{12}CO analysis done using Chan et al.'s $f(v', v'')$-values. The code currently adopts the H_2–CO collisional excitation rates from Flower & Launay (1985) and Schinke et al. (1985). Atomic H is ignored as a contributor to collisional excitation. Over most of the region rich in CO, hydrogen is expected to exist as H_2 rather than H. Our predicted excitation temperatures for $T = 20$ and 60 K and $n(H_2) = 200$ cm^{-3} agree well with the limited results published by van Dishoeck & Black (1987). Inspection of Figure 11 (*left*) shows that the solutions for $T(1, 0)$ and $T(2, 1)$ have a similar shape and do not intersect. The $T(3, 2)$ and $T(2, 1)$ solutions overlap. A compromise solution is $n_H \sim 200$ cm^{-3} and $T \sim 70$ K but solutions of higher temperature and lower density are allowed. Low-temperature models are less satisfactory because the densities required to fit $T(3, 2)$ imply an excitation temperature $T(1, 0)$ much greater than estimated from the band profiles. Our observational estimates of the excitation temperatures are based on the assumption that the two CO-containing clouds along the line of sight have identical physical conditions at all points in each cloud. This is, of course, an unlikely event. The offset of the $T(1, 0)$ locus in Figure 11 (*left*) from the other two loci suggests that one cloud dominates the absorption in the $J = 0$ lines and the other cloud in the excited rotational levels. To explore this possibility we have made a limited effort to fit the ^{12}CO band profiles using different physical conditions for the two clouds. A fair fit is found for the following conditions: $\Phi = 0.36$ with $T = 300$ K and $n_H = 60$ cm^{-3} for the more CO-rich cloud and $T = 25$ K and $n_H = 40$ cm^{-3} for the other cloud. The excitation temperatures provided by the LVG code

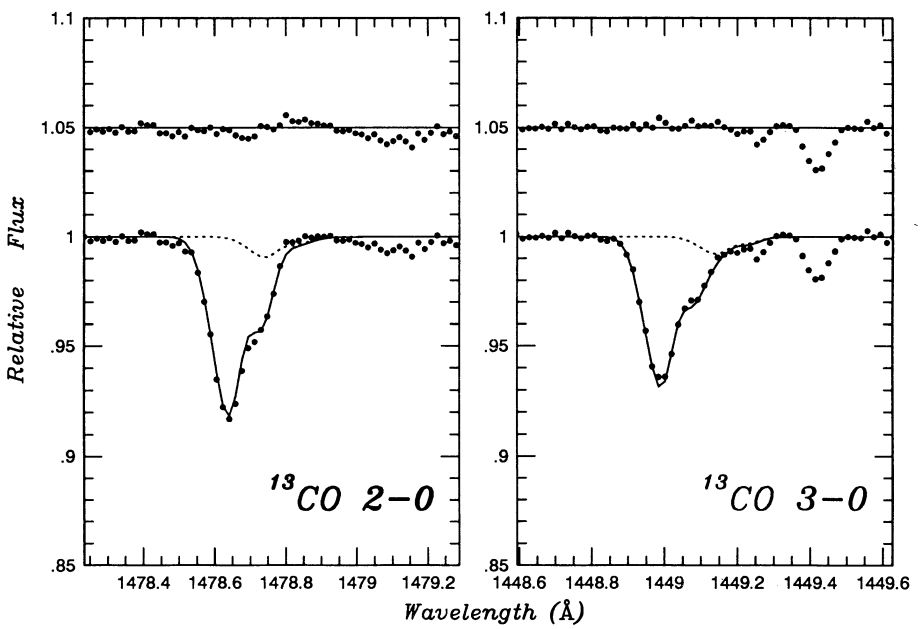

FIG. 10.—Observed and synthesized band profiles for the ^{13}CO 2–0 (*left*) and 3–0 (*right*) bands. The synthetic profiles are based on the parameters in Table 6 (see column headed "^{13}CO"). The contribution of the $^{12}C^{18}O$ lines with $^{12}C^{16}O/^{12}C^{18}O = 1550$ is represented by the dashed line. The solid line is the predicted composite of the ^{13}CO and $C^{18}O$ lines. O–C residuals are shown at an arbitrary level of 1.05 continuum units.

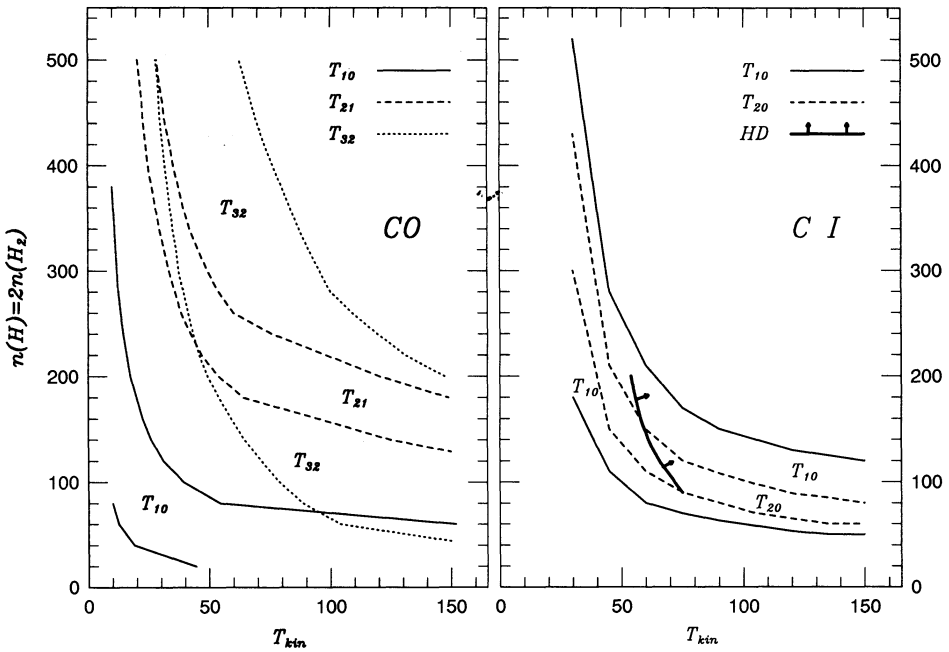

FIG. 11.—Constraints on the density (n_H) and kinetic temperature (T_{kin}) as provided by the excitation temperatures of CO (*left*) and C I (^3P) (*right*). Upper and lower constraints in the left panel are derived according to excitation temperature modeling errors, as given in Table 6. A locus from HD lines is shown in the right panel.

for these clouds give synthetic band profiles that are good fits to the observed profiles of the 6–0, 7–0, 10–0, and 11–0 bands and fair fits to the 2–0 and 3–0 bands. It is significant that the synthetic spectra reproduce well the weaker lines in all bands and, hence, the two-cloud model provides effectively rotational excitation temperatures that match those listed in Table 6 for a pair of identical clouds. The chosen cloud temperatures are consistent with the estimates $T = 340 \pm 60$ K and 80 ± 60 K made by Lambert et al. (1990) from the widths of the optical CH and CN lines.

Clearly, other diagnostics of n_H and T are also likely to be compromised by the simplifying assumption of a single set of physical conditions. Observations of line profiles with the GHRS echelles may shed more light on the differences between the physical conditions in the two "molecular" clouds. Atomic lines appear to be formed largely outside these clouds (Federman et al. 1993).

4.1.2. C I *Fine-Structure Excitation*

Analysis of excitation among the ground-state fine-structure levels of C I also provides an estimate for the density and temperature of the gas. Our analysis based on statistical equilibrium among the levels is similar to previous ones (e.g., Jenkins & Shaya 1979; Crutcher & Watson 1981), but it includes recent quantal calculations for excitation via collisions with ortho- and para-hydrogen (Schröder et al. 1991) and He (Lavendy, Robbe, & Roueff 1991; Staemmler & Flower 1991). Collisions with H (Launay & Roueff 1977) and ultraviolet pumping (Jenkins & Shaya 1979) are considered as well. The rates for excitation by proton and electron collisions are insignificant because the abundances of the charged particles are too small. As in the previous work, the astronomical results of de Boer & Morton (1979) are used for the relative populations of fine-structure levels. The solutions for the two excitation temperatures $T(1, 0) \equiv T(^3P_1, {}^3P_0)$ and $T(2, 0) \equiv T(^3P_2, {}^3P_0)$ are identical to within the observational uncertainties and in reasonable agreement with the (T, n_H) solutions from the CO excitation temperatures.

4.1.3. *Other Constraints*

To obtain more accurate separate solutions for n_H and T, one seeks a locus with a different slope to those provided by the CO and C I excitation temperatures. Crutcher & Watson (1981) in their discussion of these diagnostics considered the excitation temperature $T(1, 0)$ of the HD molecule which should be collocated with CO and C I. Crutcher and Watson's reanalysis of the observations of HD lines led to the locus shown in Figure 11. This locus differs considerably from that given by Wright & Morton (1979) because of differences in the values of the turbulent velocity assumed in the analysis of the saturated HD lines. Crutcher and Watson remark that they adopt what may be regarded as a lower bound to the turbulence and, hence their locus of n_H versus T provides a lower bound to the true locus.

Other constraints on n_H and T include the upper limit to the density set by van Dishoeck et al. (1991) from their nondetection of the $J = 3$–2 345 GHz CO line: $n_H \lesssim 425$ cm^{-3} for the stronger component and $n_H \lesssim 1250$ cm^{-3} for the weaker component on the assumption that $T \lesssim 40$ K. The n_H versus T loci from the CO and C I excitation temperatures fall below this limit (and corresponding locus) from the CO $J = 3$–2 line. Observations of interstellar C_2 lines provide an estimate of T from the population of the lowest rotational levels and an estimate of the density from the populations of the higher rotational levels. The population ratio of the two lowest levels ($J = 0$ and 2), which is well determined from observations, gives a low temperature, $T \simeq 25 \pm 10$ K (Danks & Lambert 1983; van Dishoeck & Black 1986) and sets a firm upper limit on T of 40 K (van Dishoeck & Black 1986). These estimates of T are almost independent of assumptions about the cloud and the ambient radiation field. If a higher temperature is desired in order to explain the observed fractionation of CO, one must

seek to segregate the C_2 molecules from the bulk of the CO molecules. This may be possible if the dominant component of the ultraviolet radiation field is incident upon one side of the cloud—see van Dishoeck et al. (1991, Fig. 7). The density $n_H \sim 250$ cm^{-3} (van Dishoeck et al. 1991) is based on assumptions about the cross section for collisional excitation of the C_2 rotational levels and the near-infrared radiation field. A combination of $T \sim 25$ K and $n_H \sim 250$ cm^{-3} is approximately reconcilable with the CO $T(2, 1)$ and $T(3, 2)$ temperatures.

4.2. *The ^{12}CO/^{13}CO Ratio*

Fractionation of ^{13}CO relative to ^{12}CO is measured with respect to the $^{12}CH^+/^{13}CH^+$ ratio that is generally assumed to reflect the true ^{12}C/^{13}C ratio of these diffuse clouds because the CH^+ ions are resident in warm gas and photodissociation of CH^+ is not isotopically selective. Comparison of the CH^+ absorption line profile with the CN absorption and CO emission profiles shows that the CH^+ ions are not collocated with the CO molecules. Then, in adopting $^{12}C/^{13}C \simeq 70$ from CH^+ as the reference for a discussion of fractionation of CO, one introduces the assumption that the $^{12}C/^{13}C$ ratio of the clouds containing CO is the same as in the warmer gas providing the CH^+ ions. This appears to be a safe assumption because $^{12}C/^{13}C \simeq 70$ is consistent with estimates made for local dark clouds. Atomic carbon in dark clouds is almost fully associated into CO and, hence, $^{12}C^{18}O/^{13}C^{18}O \cong {}^{12}C/^{13}C$ is expected. Emission lines of $^{12}C^{18}O$ and $^{13}C^{18}O$ are observed because they are weak and corrections for saturation may be applied reliably. Four local clouds were analyzed by Langer & Penzias (1993) who report $^{12}C/^{13}C = 57$ to 74 for a weighted average of 62 ± 4. Although clouds near ζ Oph were not in this sample, these measurements suggest that $^{12}C/^{13}C \simeq 70$, as obtained from CH^+, is likely for ζ Oph.

Fractionation is here defined by the quantity $F_{13} = (^{12}CO/^{13}CO)/(^{12}C/^{13}C)$, where the chemical symbols denote column densities and elements unsuperscripted refer to the most abundant isotope (i.e., O $\equiv$ ^{16}O). Our measurement is $^{12}CO/^{13}CO = 167 \pm 15$ and so relative to $^{12}C/^{13}C = 70$, we have $F_{13} = 2.4 \pm 0.2$. Comparable fractionation probably occurs for $^{12}C^{18}O$ relative to $^{12}C^{16}O$. Unfortunately, the $^{16}O/^{18}O$ ratio is not directly known for ζ Oph's clouds. On the assumption that $^{16}O/^{18}O = 500$, the solar value, our estimate of $^{12}C^{16}O/^{12}C^{18}O = 1550 \pm 440$ gives a fractionation $F_{18} = (^{12}C^{16}O/^{12}C^{18}O)/(^{16}O/^{18}O) = 3.1 \pm 0.9$. Our lower limit to the $^{12}C^{16}O/^{12}C^{17}O$ is adequate to show the expected fractionation of the rare $^{12}C^{17}O$ molecules (i.e., $F_{17} > 1$); the clouds are likely to have $^{16}O/^{17}O$ close to the solar value of 2600, and our limit of $^{12}C^{16}O/^{12}C^{17}O \geq 5900$ from the 2–0 band corresponds to $F_{17} \geq 2.3$.

Previous discussions of CO fractionation in diffuse clouds have identified two processes that are isotopically selective—see Paper I for references. The ion-molecular charge exchange reaction

$$^{13}C^+ + {}^{12}CO \leftrightarrow {}^{13}CO + {}^{12}C^+ + \Delta E \qquad (6)$$

favors ^{13}CO relative to ^{12}CO where $\Delta E/k = 35$ K (i.e., $F_{13} < 1$). In diffuse clouds, CO is destroyed primarily through photodissociation via ultraviolet lines—see the detailed discussion by van Dishoeck & Black (1988). This photodissociation will tend to provide $F_{13} > 1$ because the more abundant ^{12}CO is self-shielded to a greater extent than ^{13}CO. These processes of conversion and destruction compete with processes of CO formation.

According to van Dishoeck & Black (1988), CO is formed primarily through the reactions

$$C^+ + OH \rightarrow CO + H^+ \qquad (7)$$

$$\rightarrow CO^+ + H\,, \qquad (8)$$

where CO^+ is converted to CO through

$$CO^+ + H_2 \rightarrow HCO^+ + H \qquad (9)$$

and

$$HCO^+ + e \rightarrow CO + H\,. \qquad (10)$$

On the plausible assumption that these reactions are blind to the isotopic form of C or O, the ratio of ^{12}CO and ^{13}CO in equilibrium is given by (see Paper I)

$$\frac{n(^{12}CO)}{n(^{13}CO)} = \frac{n(^{12}C^+)}{n(^{13}C^+)} \frac{\Gamma_{13} + n(^{12}C^+)k_1^r}{\Gamma_{12} + n(^{12}C^+)k_1^f}\,, \qquad (11)$$

where n denotes the local density, Γ_i (s^{-1}) is the photodissociation rate ($i = 12$ for ^{12}CO, $i = 13$ for ^{13}CO), and k_1^f and k_1^r are the rates for reaction (6) in the forward and reverse directions, respectively. In diffuse clouds, one supposes that the C^+ ions are not fractionated and then equation (11) corresponds to

$$F_{13} = \frac{\Gamma_{13} + n(^{12}C^+)k_1^r}{\Gamma_{12} + n(^{12}C^+)k_1^f}\,. \qquad (12)$$

If isotopic charge exchange occurs at a much faster rate than photodissociation, equation (2) simplifies to

$$F_{13} = \frac{k_1^r}{k_1^f} = \exp\left(-\frac{35}{T}\right) \qquad (13)$$

and $F_{13} < 1$ in contrast to the observed value $F_{13} = 2.4$. For example, at the temperature $T \simeq 25$ K suggested by the C_2 lines, $F_{13} \simeq 0.2$. At $T = 80$ and 300 K, $F_{13} \simeq 0.6$ and 0.9 respectively. Note that, as long as equilibrium is attained, F_{13} from equation (13) depends only on the ratio of the rate constants k_1^r and k_1^f and, hence, on ΔE.

If photodissociation destroys CO molecules much more rapidly than the isotopic charge exchange reaction swaps ^{12}C for ^{13}C and vice versa, equation (12) simplifies to

$$F_{13} = \frac{\Gamma_{13}}{\Gamma_{12}}\,. \qquad (14)$$

At the surface of a diffuse cloud, $\Gamma_{13} \cong \Gamma_{12}$ (see van Dishoeck & Black 1988) and $F_{13} \simeq 1$. The higher optical depths in ^{12}CO ultraviolet lines means that, in the interior of a cloud, the radiation field is more severely reduced at the wavelengths leading to ^{12}CO photodissociation than at the wavelengths causing ^{13}CO photodissociation. The molecule ^{12}CO is said to provide self-shielding in diffuse clouds. Under these conditions $\Gamma_{13} > \Gamma_{12}$ and $F_{13} > 1$.

Photodissociation rates Γ_i may be estimated from van Dishoeck & Black (1988). There are three principal ingredients to a calculation of Γ_i: the incident radiation field, the cloud geometry, and the photodissociation cross sections of the individual transitions. The ratio Γ_{13}/Γ_{12} is largely independent of the incident radiation field and the cross sections of the individual transition but is primarily dependent on "the geometry," i.e., the effect of self-shielding for ^{12}CO. van Dishoeck & Black (1988, their eq. [3] and Table 5) give estimates of Γ_{12} and Γ_{13} for a uniform slab illuminated by

Draine's (1978) radiation field. It is possible from their estimates to find Γ_{13}/Γ_{12} for different depths into the cloud.

Depths are here specified by the ^{12}CO column density from the illuminated boundary. At $N(^{12}\mathrm{CO}) \simeq 2.5 \times 10^{15}$ cm^{-2} and $N(^{13}\mathrm{CO}) = N(^{12}\mathrm{CO})/170 = 1.5 \times 10^{13}$ cm^{-2}, $F_{13} = \Gamma_{13}/\Gamma_{12} \simeq 3.6$. In the considered geometry, this is the maximum value of Γ_{13}/Γ_{12} because at smaller CO column densities (i.e., at points closer to the illuminated boundary), the self-shielding is less effective and Γ_{13}/Γ_{12} tends to unity at the boundary: we estimate $\Gamma_{13}/\Gamma_{12} \sim 3.3$ and 2.7 at CO column densities of one-half and one-quarter, respectively, of the observed value. These estimates of Γ_{13}/Γ_{12} suggest that it may be possible to maintain the necessary average $F_{13} \simeq \Gamma_{13}/\Gamma_{12} \sim 2.4$ over the line of sight to match the observed fractionation. van Dishoeck & Black (1988) assert or imply that the rates are insensitive to the assumed *b*-values, excitation temperature, and the scattering properties of the dust. The calculations would seem most applicable if ζ Oph is the primary source of ultraviolet radiation. On the other hand, the effect of self-shielding can be increased if our line of sight to ζ Oph runs approximately perpendicular to the line from the cloud to the primary source of ultraviolet radiation. Then, the ^{12}CO column density seen by the ultraviolet radiation may be larger than along the line of sight. A calculation by van Dishoeck & Black (1988, their Fig. 5) suggests $\Gamma_{13}/\Gamma_{12} \sim 6$ is attainable over large distances into the cloud as measured along the line of sight from the illuminating star. Since this increase of Γ_{13}/Γ_{12} is paired with a reduction of both Γ_{12} and Γ_{13}, photodissociation is reduced in importance relative to the isotopic charge exchange which may then control the fractionation and give $F_{13} < 1$ contrary to the observed value. In fact, the ^{12}C^{18}O molecule carries information about the efficacy of CO self-shielding.

Since the O atoms in the clouds are predominantly neutral, ^{12}C^{18}O and ^{12}C^{16}O are not fractionated by the analog of reaction (6), i.e., $^{18}\mathrm{O}^+ + {}^{12}\mathrm{C}^{16}\mathrm{O} \leftrightarrow {}^{12}\mathrm{C}^{18}\mathrm{O} + {}^{16}\mathrm{O}^+$. Then, $F_{18} = \Gamma_{18}/\Gamma_{16} = 1$. For conditions such that the key ultraviolet transitions of ^{13}C^{16}O are optically thin, we expect $\Gamma_{13} \cong \Gamma_{18}$ and $F_{18} \cong \Gamma_{13}/\Gamma_{16}$ which is also F_{13} in the limit that photodissociation is faster than isotopic charge exchange. van Dishoeck & Black's (1988, their Table 5) calculations show that Γ_{18} exceeds Γ_{13} by about 10% at the point in the cloud where $N(\mathrm{CO}) = 2.6 \times 10^{15}$ cm^{-2} to the illuminated boundary. Averaged over the entire path length Γ_{18} and Γ_{13} will be equal to within a few percent. In the case of an illuminating star approximately perpendicular to the line of sight, Γ_{18} may exceed Γ_{13} by a factor of 2 (van Dishoeck & Black 1988, their Fig. 5*a*). Unfortunately, it is presently difficult to make full use of the ^{12}C^{18}O lines because they are blended with the stronger ^{13}C^{16}O lines: we set $F_{18} \simeq 3$. In Paper I, the ECH-A spectra on which ^{12}C^{18}O lines are well resolved, the low S/N of the available spectra of the 5–0 and 6–0 bands enabled us to set the limit $F_{18} \gtrsim 1.6$. If $F_{18} \simeq 3$, and $\Gamma_{18} \simeq \Gamma_{13}$ is supposed, the observed $F_{13} = 2.4$ is accounted for provided that photodissociation is faster than the isotopic charge exchange.

This provision is not satisfied by ζ Oph's clouds as they are usually modeled. That the isotopic charge exchange ameliorates the selective effects of photodissociation is clearly demonstrated by van Dishoeck & Black's (1988, their Table 6) predictions of CO column densities for cloud models that reproduce many of the observed atomic and molecular column densities. For our models with a central density $n_{\mathrm{H}} = 350$ cm^{-3} and a central temperature $T = 30$ K and cloud envelopes of lower density and warmer temperatures, the predicted ratio is $^{12}\mathrm{CO}/^{13}\mathrm{CO} = 44$–$56$ for the assumed ratio $^{12}\mathrm{C}/^{13}\mathrm{C} = 45$, i.e., $F_{13} \lesssim 1.2$; a slight increase in F_{13} is expected for an assumed $^{12}\mathrm{C}/^{13}\mathrm{C} = 70$. In a fifth model, the C^+ column density was lowered by introducing large C-containing molecules and then $^{12}\mathrm{CO}/^{13}\mathrm{CO} = 74$ or $F_{13} = 1.6$ was predicted. The predicted F_{13} will increase somewhat above 1.6 for $^{12}\mathrm{C}/^{13}\mathrm{C} \simeq 70$. The reduction of the C^+ density improved the match to the observed C^+ column density and reduced the effectiveness of the isotopic charge exchange reaction. Since the C^+ density might be reduced further, and the incident radiation field increased or the dust opacity reduced at the wavelengths ($\lambda \lesssim 1000$ Å) responsible for CO dissociation, the observed $F_{13} = 2.4$ may not be out of reach of acceptable revisions to the models considered by van Dishoeck & Black (1988).

To illustrate the possibilities, we estimated Γ_{12} and Γ_{13} for a uniform slab using van Dishoeck & Black's (1988) Table 5, a ratio $^{12}\mathrm{CO}/^{13}\mathrm{CO} = 170$, and the assumption that the dust optical depth varies linearly with CO column density. We assume the slab is illuminated by ζ Oph on one side. Equation (12) may be written as

$$F_{13} = \frac{\Gamma_{13}}{\Gamma_{12}}\left[1 + \frac{3.2 \times 10^{-12}}{\Gamma_{13}}\left(\frac{n_{\mathrm{H}}}{200}\right)\left(\frac{\delta_{\mathrm{C}}}{0.1}\right)\right] \times \left[1 + \frac{6.4 \times 10^{-12}}{\Gamma_{12}}\left(\frac{n_{\mathrm{H}}}{200}\right)\left(\frac{\delta_{\mathrm{C}}}{0.1}\right)\right]^{-1}, \quad (15)$$

where we assume $T = 50$ K, a solar C abundance, and adopt the rates k_1^r and k_1^f from Smith & Adams (1980). The factor δ_{C} (< 1) recognizes that carbon is depleted onto grains and some gaseous carbon atoms will not be ionized: the factor $\delta_{\mathrm{C}} \simeq 0.1$ is at the low end of previous estimates for the line of sight. A density $n_{\mathrm{H}} = 200$ cm^{-3} is consistent with the diagnostics displayed in Figure 11. The photodissociation rates Γ_i are subject to a scaling factor I_{UV} which is the factor by which the ultraviolet radiation field differs from that proposed by Draine (1978): van Dishoeck & Black (1988) adopt $I_{\mathrm{UV}} = 3.5$ for ζ Oph. For a uniform slab with $n_{\mathrm{H}} = 200$ cm^{-3} and $T = 50$ K and illuminated on one side with a radiation field corresponding to $I_{\mathrm{UV}} = 3.5$, we find the local fractionation to be $F_{13} = 1.3$, 1.9, 2.7, and 2.6 at CO column densities corresponding to $N/2.5 \times 10^{15} = 1$, 0.75, 0.5, and 0.25, respectively but declining to $F_{13} = 1.0$ at $N = 0$. For this example, it is evident that F_{13} averaged over the path length will be close to the observed value. (Recall that the ^{13}CO molecules reside in more turbulent gas than the bulk of the ^{12}CO molecules. This difference will tend to increase F_{13}.) This explanation of the observed F_{13} is dependent, of course, on the assumption that $\delta_{\mathrm{C}} = 0.1$, $n_{\mathrm{H}} = 200$ cm^{-3}, and $T = 50$ K. A concern must be that $\delta_{\mathrm{C}} = 0.1$ is too low because the ionization of carbon is likely to be effectively complete over much of the path and the observed depleion of C corresponds to $\delta_{\mathrm{C}} \simeq 0.4$ not 0.1 (Cardelli et al. 1993). Perhaps, this concern may be alleviated by the recognition that one molecular component may be quite warm. Recall that our preliminary fit of the CO bands using two clouds have $T = 300$ K and $n_{\mathrm{H}} \simeq 60$ cm^{-3} for a warmer component and $T = 25$ K and $n_{\mathrm{H}} \simeq 40$ cm^{-3} for the cooler component. At these densities, the isotopic charge exchange reaction can be of minor importance and, at $T = 300$ K, the reaction is ineffective in producing fractionation and serves only to dilute the effects of photodissocation.

It remains to be shown whether these variations of the standard models account satisfactorily for other atomic and molecular lines. For standard models, it is apparent that, as van

Dishoeck and Black's quantitative predictions for ζ Oph model clouds demonstrate, it is by no means a trivial task to account for the observed fractionation ($F_{13} = 2.4$) with the present chemical network in which isotropic charge exchange competes with photodissociation in fractionating $^{13}C^{16}O$ relative to $^{12}C^{16}O$ under the physical conditions thought to exist in these diffuse clouds. The question arises: does this difficulty arise because the chemical network is defective or because the physical conditions and cloud geometry differ from those identified?

4.3. *The CO Column Density*

A discussion of fractionation of $^{13}C^{16}O$ relative to $^{12}C^{16}O$ would be incomplete without reference to the puzzle provided by the observed column density of $^{12}C^{16}O$ along the line of sight to ζ Oph. Proposed solutions to this puzzle should not aggravate the difficulty in accounting for the observed fractionation. Perhaps, the solution to the puzzle offered by the CO column density is the key or related to the key to the fractionation puzzle.

Our earlier reference to van Dishoeck & Black's (1988) models of the ζ Oph cloud was limited to their predictions for the ratio F_{13}. Inspection shows, as van Dishoeck and Black acknowledge, that the predicted column density of ^{12}CO is about an order of magnitude less than the observed value. The models constructed by van Dishoeck and Black for other diffuse clouds show a similar discrepancy and thus the discrepancy in the case of ζ Oph cannot be attributed to a unique geometry for this line of sight. The solution would seem to lie in either the design or implementation of the adopted chemical network.

van Dishoeck and Black base their calculations on formation of CO by the reactions (7) through (10). The models are constructed to reproduce the observed OH column density that is key to the initiating reaction (7). It is asserted that neither the omission of other chemical reactions (e.g., $O + CH \rightarrow CO + H$) nor the neglect of the production of CO on grain surfaces will account for the order of magnitude discrepancy. van Dishoeck and Black suggest that the discrepancy is "most likely caused by an overestimate of the CO photodissociation rate" but a cut of this rate by an order of magnitude will further enhance the role of the isotopic charge exchange in the fractionation and ensure that $F_{13} < 1$ is predicted in violation of our observations. It matters little how the rate is cut. The cut can probably not be achieved by reducing the photodissociation cross sections of CO because they are thought to be accurate to at least a factor of 2; these inaccuracies probably have a smaller influence on the ratio Γ_{13}/Γ_{12} that helps determine the fractionation F_{13}. A cut in the interstellar radiation field incident upon the clouds or changes to the properties of the dust grains affecting the radiation field within the clouds seems unlikely to affect greatly the ratio Γ_{13}/Γ_{12}. In short, while reduction of the photodissociation rate may bring predicted and observed column densities of CO into accord, its effect on the predicted F_{13} will be severe unless a compensating isotopically dependent change can be identified.

On the other hand, a modest increase of the photodissociation rates, which would make it easier to reconcile the observed and predicted F_{13}, does not necessarily have to increase the discrepancy between the observed and predicted CO column densities. We note that the CO production rates considered by van Dishoeck and Black are based on an estimate of the rate constant for (7) of (apparently) 7.7×10^{-10} $cm^3\ s^{-1}$ but a rate constant as high as 2.9×10^{-9} $cm^3\ s^{-1}$ is not excluded (Federman & Huntress 1989). If this possible factor of 4 increase were matched by a factor of 4 increase in Γ_i, it would be easier to account for F_{13}; the factor of 10 discrepancy in the predicted and observed CO column densities would remain, of course. Perhaps, the other chemical pathways ignored by van Dishoeck and Black do contribute. We assume that the formation reactions are not isotopically selective.

A common but not a universal assumption is that the chemistry in diffuse clouds attain equilibrium. The populations of the excited rotational levels of the H_2 molecule are used by van Dishoeck and Black (and others) to constrain the intensity of the ultraviolet radiation field; the levels in question are populated by cascades from excited states fed by ultraviolet absorption lines. The H_2 molecules are formed on grain surfaces and probably on ejection have a high excitation temperature. Relaxation of the initial distribution of H_2 molecules among rotational levels occurs slowly. In equilibrium calculations, the rotational temperature of H_2 is assumed to have relaxed to the equilibrium value which then provides the estimate of I_{UV}. Wagenblast (1992) models the formation and rotational relaxation of H_2 molecules in a cloud initially composed of atomic hydrogen. He shows that his models in their slow approach to H_2 rotational equilibrium can account for the column densities of rotationally excited H_2 and of many other molecules, atoms and ions including CO. It would appear that the CO column density is successfully accounted for because his ultraviolet radiation field is less intense than that adopted by van Dishoeck and Black: $I_{UV} = 1/10$ rather than $I_{UV} = 3.5$. Wagenblast's calculations allow a low value of I_{UV} because the ultraviolet radiation field is not the sole factor controlling the population of the excited levels of the H_2 molecules. Wagenblast assumes a cloud density of 240 cm^{-3} and a temperature of 140 K on the irradiated half and 30 K on the other half. This solution to the problem of the CO column density most probably hampers a reconcilation of the predicted and observed fractionation because the role of the isotopic charge exchange reaction is supreme when I_{UV} is cut to 1/10. This reaction achieves equilibrium in a time short compared to that required for the H_2 molecules to reach rotational equilibrium.

If destruction of CO by photodissociation is supplemented by chemical reactions, it is yet more difficult to account for both the fractionation and the CO column density. For example, $He^+ + CO \rightarrow C^+ + O + He$ may dominate CO destruction in dark clouds where the cosmic rays ionize He (and other atoms). Additions of this reaction to our scheme corresponds to adding the same term to the numerator and the denominator of the right-hand side of equation (11) and the isotopically selective effect of photodissociation is diluted and an explanation for the observed F_{13} made more difficult. It would seem that the only way to match the observed CO column density and observed fractionation is to introduce more efficient modes of CO formation. It would probably ease the task of accounting for the fractionation if the photodissociation rate were increased by a modest factor and the formation rates then need to be further increased to compensate. It seems unlikely that the rate constant for the isotopic charge exchange reaction is in error by a significant amount (see Smith & Adams 1980). We have not identified an isotopically sensitive process to assist photodissociation in offsetting the effect of the isotopic charge exchange reaction in driving F_{13} below unity. Cloud geometry is important because it is the self-shielding of ^{12}CO that drives the ratio Γ_{13}/Γ_{12} greater than unity. Present models of homogeneous clouds do not

consider the recent discovery that CO and other molecules are found in two clouds and not a single cloud. Our discovery that the ^{13}CO molecules reside in a more turbulent region than the bulk of the ^{12}CO molecules further attests to the complexity of the clouds. These factors could conceivably lead to increases of Γ_{13}/Γ_{12} and increase the fractionation for a given average density and temperature.

5. CONCLUDING REMARKS

This analysis of high S/N GHRS grating spectra of CO A–X bands confirms our earlier result (Paper I) based on low S/N echelle spectra: interstellar CO toward ζ Oph is severely fractionated. We find that the rare isotopic species $^{13}C^{16}O$, $^{12}C^{17}O$, and $^{12}C^{18}O$ are underabundant by at least a factor of 2.2 with respect to the measured or inferred atomic isotopic ratios. For example, $^{12}CO/^{13}CO \simeq 170$ but $^{12}C/^{13}C = 70$ as measured from the CH^+ optical lines. These observations of fractionation appear to require revisions to standard models of the ζ Oph cloud(s) (e.g., van Dishoeck & Black 1986, 1988) in order that photodissociation of CO and not the isotopic charge exchange reaction be the controlling influence on the isotopic fractionation of CO.

We thank N. J. Evans II for the LVG code. David L. Lambert and Yaron Sheffer were supported in part by NASA contract NAG5-1616.

REFERENCES

Bagnuolo, W. G., Jr., & Gies, D. R. 1991, ApJ, 376, 266
Cardelli, J. A., Mathis, J. S., Ebbets, D. C., & Savage, B. D. 1993, ApJ, 402, L17
Cardelli, J. A., Savage, B. D., & Ebbets, D. C. 1991, ApJ, 383, L23
Cayrel, R. 1988, in The Impact of Very High S/N Spectrocopy on Stellar Physics, ed. G. Cayrel de Strobel & M. Spite (Dordrecht: Kluwer), 345
Chan, W. F., Cooper, G., & Brion, C. E. 1993, Chem. Phys., 170, 123
Crane, P., Hegyi, D. J., & Lambert, D. L. 1991, ApJ, 378, 181
Crutcher, R. M., & Watson, W. D. 1981, ApJ, 244, 855
Danks, A. C., & Lambert, D. L. 1983, A&A, 242, 424
de Boer, K. S., & Morton, D. C. 1979, A&A, 71, 141
De Leon, R. L. 1988, J. Chem. Phys., 89, 20
———. 1989, J. Chem. Phys., 51, 5859
Draine, B. T. 1978, ApJS, 36, 595
Eidelsberg, M., Rostas, F., Breton, J., & Thieblemont, B. 1992, J. Chem. Phys., 96, 5585
Federman, S. R., & Huntress, W. T., Jr. 1989, ApJ, 338, 140
Federman, S. R., Sheffer, Y., Lambert, D. L., & Gilliland, R. L. 1993, ApJ, 413, L51
Field, R. W., Benoist d'Azy, O., Lavollée, M., Lopez-Delgado, R., & Tramer, A. 1983, J. Chem. Phys., 78, 2838
Flower, D. R., & Launay, J. M. 1985, MNRAS, 214, 271
Gilliland, R. L., Morris, S. L., Weymann, R. J., Ebbets, D. C., & Lindler, D. J. 1992, PASP, 104, 367
Haridass, C., & Huber, K. P. 1994, ApJ, in press
Jansson, P. A. 1984, Deconvolution With Applications in Spectroscopy (New York: Academic)
Jenkins, E. B., Drake, J. F., Morton, D. C., Rogerson, J. B., Spitzer, L., & York, D. G. 1973, ApJ, 181, L122
Jenkins, E. B., & Shaya, E. J. 1979, ApJ, 231, 55
Lambert, D. L., Sheffer, Y., & Crane, P. 1990, ApJ, 359, L19
Langer, W. D., & Penzias, A. A. 1993, ApJ, 408, 539
Lassettre, E. N., & Skerbele, A. 1971, J. Chem. Phys., 54, 1597
Launay, J. M., & Roueff, E. 1977, A&A, 56, 289
Lavendy, H., Robbe, J. M., & Roueff, E. 1991, A&A, 241, 317
Le Bourlot, J., Gerin, M., & Perault, M. 1989, A&A, 219, 179
Meyer, V. D., & Lassettre, E. N. 1971, J. Chem. Phys., 54, 1608
Reader, J., Acquista, N., Sansonetti, C. J., & Sansonetti, J. 1989, Spectrum of a Platinum/Neon Hollow Cathode Lamp from 1032 to 4100 Å (Gaithersburg: National Inst. Standards and Technology)
Schinke, R., Engle, V., Buck, U., Meyer, H., & Diercksen, G. H. F. 1985, ApJ, 299, 939
Schröder, K., Staemmler, V., Smith, M. D., Flower, D. R., & Jaquet, R. 1991, J. Phys. B., 24, 2487
Sheffer, Y., Federman, S. R., Lambert, D. L., & Cardelli, J. A. 1992, ApJ, 397, 482 (Paper I)
Smith, D., & Adams, N. G. 1980, ApJ, 242, 424
Snell, R. L. 1981, ApJS, 45, 121
Staemmler, V., & Flower, D. R. 1991, J. Phys. B., 24, 2343
Stahl, O., & Wilson, T. L. 1992, A&A, 254, 327
Stahl, O., Wilson, T. L., Henkel, C., & Appenzeller, I. 1989, A&A, 221, 321
van Dishoeck, E. F., & Black, J. H. 1986, ApJ, 307, 332
———. 1987, in Physical Processes in Interstellar Clouds, ed. G. E. Morfill & M. Scholer (Dordrecht: Reidel), 241
———. 1988, ApJ, 334, 771
van Dishoeck, E. F., Black, J. H., Phillips, T. G., & Gredel, R. 1991, ApJ, 366, 141
Wagenblast, R. 1992, MNRAS, 259, 155
Wannier, P. G., Penzias, A. A., & Jenkins, E. B. 1982, ApJ, 254, 100 (WPJ)
Wilson, T. L., Mauersberger, R., Langer, W. D., Glassgold, A. E., & Wilson, R. W. 1992, A&A, 262, 248
Wright, E. L., & Morton, D. C. 1979, ApJ, 227, 483